



Long-Baseline Neutrino Oscillation Experiments

Citation

Feldman, G. J., J. Hartnell, and T. Kobayashi. 2013. "Long-Baseline Neutrino Oscillation Experiments." *Advances in High Energy Physics* 2013: 1–30. doi:10.1155/2013/475749.

Published Version

doi:10.1155/2013/475749

Permanent link

<http://nrs.harvard.edu/urn-3:HUL.InstRepos:28237456>

Terms of Use

This article was downloaded from Harvard University's DASH repository, and is made available under the terms and conditions applicable to Open Access Policy Articles, as set forth at <http://nrs.harvard.edu/urn-3:HUL.InstRepos:dash.current.terms-of-use#OAP>

Share Your Story

The Harvard community has made this article openly available.
Please share how this access benefits you. [Submit a story](#).

[Accessibility](#)

Long-baseline Neutrino Oscillation Experiments

G. J. Feldman

Department of Physics, Harvard University, Cambridge, Massachusetts 02138, USA.

E-mail: gfeldman@fas.harvard.edu

J. Hartnell

Department of Physics and Astronomy, University of Sussex, Brighton. BN1 9QH. United Kingdom.

E-mail: j.j.hartnell@sussex.ac.uk

T. Kobayashi

Institute for Particle and Nuclear Studies, High Energy Accelerator Research Organization (KEK), 1-1, Oho, Tsukuba, 305-0801, Japan.

E-mail: takashi.kobayashi@kek.jp

Abstract. A review of accelerator long-baseline neutrino oscillation experiments is provided, including all experiments performed to date and the projected sensitivity of those currently in progress. Accelerator experiments have played a crucial role in the confirmation of the neutrino oscillation phenomenon and in precision measurements of the parameters. With a fixed baseline and detectors providing good energy resolution, precise measurements of the ratio of distance/energy (L/E) on the scale of individual events have been made and the expected oscillatory pattern resolved. Evidence for electron neutrino appearance has recently been obtained, opening a door for determining the CP violating phase as well as resolving the mass hierarchy and the octant of θ_{23} : some of the last unknown parameters of the standard model extended to include neutrino mass.

1. Introduction

Neutrino oscillation experiments are normally categorized into short-baseline and long-baseline experiments. For experiments using accelerator neutrinos as the source, the long-baseline means that $E/L \simeq \Delta m^2 \sim 2.5 \times 10^{-3} \text{ eV}^2$, where E and L are the neutrino energy and flight distance respectively. In this article, accelerator long-baseline (LBL) neutrino oscillation experiments are reviewed. The recent reactor neutrino experiments to look for non-zero θ_{13} at $\Delta m^2 \sim 2.5 \times 10^{-3} \text{ eV}^2$ and atmospheric neutrino experiments are covered elsewhere in this Special Issue on Neutrino Physics.

Neutrino beams for the LBL experiments are produced in the “conventional” method where a high energy proton beam hits a target and the pions that are produced then decay in flight to give muon neutrinos. The typical neutrino energy thus produced is 0.5–10 GeV and that sets the necessary distance to a neutrino detector to be several hundreds of kilometers such that the

neutrino oscillation driven by $\Delta m^2 \sim 2.5 \times 10^{-3} \text{ eV}^2$ can be investigated. This review describes KEK [1], NuMI [2], CNGS [3] and J-PARC [4] neutrino beams and their associated experiments.

The goals of the first LBL experiments proposed in 1990s, K2K [5], MINOS [6] and CERN to Gran Sasso (CNGS) experiments OPERA [7] and ICARUS [8] were to clarify the origin of the anomaly observed in the atmospheric neutrino measurements of Kamiokande [9] and IMB [10] and later to confirm the discovery of neutrino oscillations by Super-Kamiokande (SK) in 1998 [11]. Kamiokande observed a deficit of muon neutrinos coming through the earth, which could have been interpreted as muon to tau neutrino oscillation and/or to electron neutrino oscillation. Soon afterwards, the CHOOZ experiment [12] excluded the possibility that muon to electron neutrino oscillation is the dominant mode. Therefore, the goal of the first generation LBL experiments was focused on confirming muon to tau neutrino oscillation. The K2K and MINOS experiments, which used beams with neutrino energies of a few-GeV, focused on detecting muon neutrino disappearance because the energy of the neutrinos was rarely high enough to make ν_τ charged current interactions (threshold energy is about 3.5 GeV). In contrast, the CNGS experiments make use of a higher energy (~ 20 GeV) neutrino beam and OPERA is optimized for the detection of tau neutrino appearance.

Soon after the discovery of neutrino oscillation by SK, the importance of the sub-leading electron neutrino appearance channel was pointed out. In the three flavor mixing picture, the probability of electron neutrino appearance gives a measure of the mixing angle θ_{13} . The existence of electron neutrino appearance at the atmospheric oscillation length means non-zero θ_{13} . Only an upper bound of $\sin^2(2\theta_{13}) = 0.14$ (90% C.L.) from the CHOOZ experiment was known until very recently. Because the CP violating observable, the phase δ , appears always in the product with $\sin(2\theta_{12}) \sin(2\theta_{23}) \sin(2\theta_{13})$ and θ_{23} and θ_{12} are known to be large, the size of θ_{13} is a major factor in the feasibility of the future CP violation search.

With the goal to discover electron neutrino appearance and determine θ_{13} , the T2K experiment [4] in Japan started taking data in 2010 and the NO ν A experiment [13, 14, 15] in the USA is now under construction and will start measurements in 2013. The design of these experiments was optimized for detection of electron neutrino appearance. Both T2K and NO ν A adopted a novel “off-axis” beam technique that provides a narrow peak in the energy spectrum, tuned to be at the expected oscillation maximum, while at the same time reducing the unwanted high energy tail. The $\nu_\mu \rightarrow \nu_e$ transition is a sub-dominant effect and the oscillation probability to be probed is small. To have enough sensitivity, beam powers of order 1 MW and detector masses of order 10 kilotons are required and as such these experiments are sometimes called “superbeam” experiments.

With evidence of ν_e appearance from early T2K results and the recent measurement of $\bar{\nu}_e$ disappearance by the reactor experiments [16, 17, 18], the major focus for the future will be to determine the mass hierarchy and search for evidence of CP violation. NO ν A will have the longest baseline of all second-generation experiments at 810 km, which will give enhanced sensitivity to the neutrino mass hierarchy due to the neutrino-matter interaction in the Earth as the neutrinos propagate. Information on the mass hierarchy and the expected precision measurement of θ_{13} from the reactor experiments will be crucial to resolve degeneracies in the grand combination of T2K, NO ν A and reactor experiments to reveal information on what nature has chosen for leptonic CP violation.

Beyond oscillations, the provision of intense and relatively well understood neutrino beams along with the large detectors in these experiments has opened up whole new avenues to look for new physics. This review provides a concise overview of searches for sterile neutrinos, velocity measurements of neutrinos and searches for violation of Lorentz symmetry. In the future, the MINOS+ experiment [19] will focus on searches for new physics through high-precision, high-statistics measurements with the NuMI beam operating at a peak on-axis energy of 7 GeV.

This review paper is structured as follows. Section 2 describes the beams and section 3 gives

an overview of the detectors. The results from long-baseline neutrino oscillation experiments are presented here in three parts: section 4 describes the measurements made using the dominant $\nu_\mu \rightarrow \nu_\tau$ oscillation mode; section 5 details the recent detection of sub-dominant $\nu_\mu \rightarrow \nu_e$ oscillations; and section 6 describes the results from searches for new physics such as sterile neutrinos. Future sensitivities are described in section 7 and a conclusion is given in section 8.

2. Neutrino Beams

The accelerator neutrino beams used by the experiments covered in this review article are described in this section. As in other areas of particle physics, the experiments' detectors exist in a strongly coupled relationship with the beam and it is important to consider both beam and detector to understand the design and performance of the experiments.

An interesting feature of neutrino beams is that multiple detectors can be simultaneously exposed to the same individual beam spills with no noticeable effect on the beam itself. This is true for Near and Far detectors but also, for example, where there are multiple experiments in the same underground laboratory.

An advantage of accelerator beams is the ability to exploit the pulsed nature of the beams to reject backgrounds from cosmic rays and atmospheric neutrinos. With beam pulses lasting tens of microseconds and accelerator cycle times measured in seconds, a background rejection factor of 10^5 is typical.

The beams used in long-baseline experiments are described here in the following order: section 2.1 describes the beam used by K2K; section 2.2 describes the NuMI beam used by MINOS and in future NO ν A and MINOS+; section 2.3 describes the CNGS beam used by OPERA and ICARUS; and section 2.4 describes the J-PARC beam used by T2K.

2.1. KEK Beam

In this section, the beam for the first LBL experiment K2K in Japan which was in operation from 1999 to 2004 is described [5]. A schematic layout of the K2K beam line is shown in Figure 1. The beam of muon neutrinos was produced with the KEK 12 GeV proton synchrotron (PS) and was sent towards Super-Kamiokande, which is located 250 km from KEK. The central axis of the neutrino beam was aligned to aim at the center of Super-Kamiokande giving an on-axis wideband beam.

The proton beam was extracted from the PS in a single turn with a 2.2 s cycle time. The spill was 1.1 μ s long and consisted of nine bunches. The proton beam intensity reached about 6×10^{12} protons/pulse, corresponding to a beam power of about 5 kW.

Initially the target was a 66 cm long, 2 cm diameter Al rod but this was replaced with a wider, 3 cm diameter rod in November 1999. Secondary positive pions were focused by two electromagnetic horns [20]. Both horns had a pulsed current about 1 ms long with a 200 kA peak for the June 1999 run, and that was increased to a 250 kA peak for runs after November 1999. The target was embedded in the first horn and played a role as an inner conductor as shown in Figure 2.

Measurements of the momenta and angular distribution of secondary pions, $N(p_\pi, \theta_\pi)$, were made using the pion monitor. This detector was a gas Čerenkov detector occasionally placed just downstream of the second horn in the target station. The results of the pion monitor measurements were used in calculations of the ratio of the flux at SK to the flux at the near detector (ND), $R_\Phi(E_\nu) \equiv \Phi_{\text{SK}}(E_\nu)/\Phi_{\text{ND}}(E_\nu)$.

The target region was followed by a 200 m long decay pipe where pions decayed in flight to muon neutrinos and muons. At the downstream end of the decay pipe, there was a beam dump made of iron 3 m thick and followed by 2 m thick concrete. Muons above 5 GeV could penetrate the beam dump and be detected by the muon monitors installed just behind the beam dump.

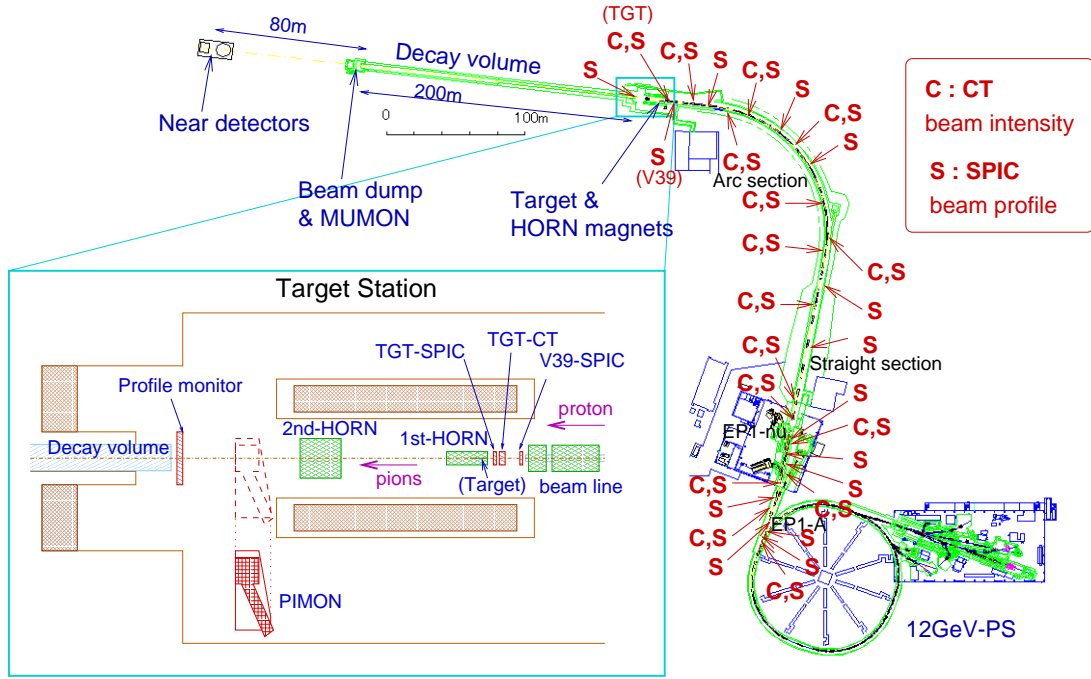


Figure 1. A schematic of the K2K beamline that includes the primary proton beamline.

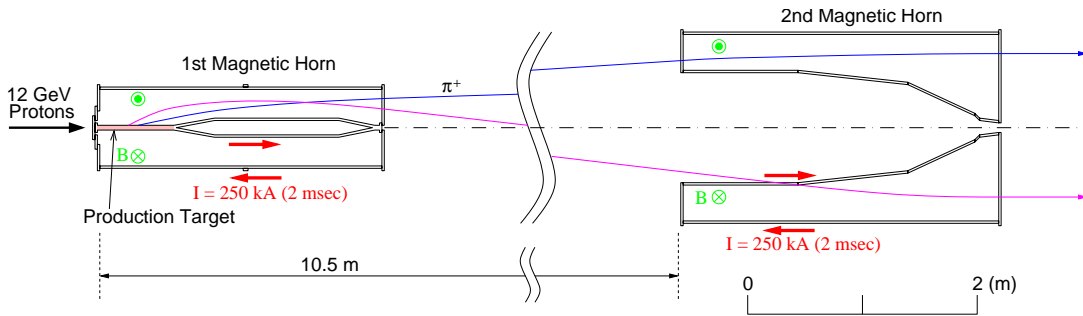


Figure 2. A schematic showing the layout and operation of the K2K beamline target and horns.

The muon monitors consisted of $2\text{ m} \times 2\text{ m}$ segmented ionization chambers along with an array of silicon pad detectors and provided spill-by-spill monitoring of the beam profile and intensity.

Beam line components were aligned with Global Positioning System (GPS) [21]. The alignment uncertainty from the GPS survey was $\lesssim 0.01\text{ mrad}$ while that of the civil construction was $\lesssim 0.1\text{ mrad}$, both of which were much better than physics requirement of 1 mrad .

The expected neutrino spectra at SK are plotted in Figure 3. The average neutrino energy was 1.3 GeV and the purity of ν_μ in the beam was estimated by Monte Carlo (MC) simulation to be 98.2% and ν_e contamination to be 1.3% .

The K2K experiment started physics data taking in June 1999 and finished in November 2004. The total number of protons on target (POT) delivered was 1.049×10^{20} , of which 0.922×10^{20} POT were used in the final physics analysis.

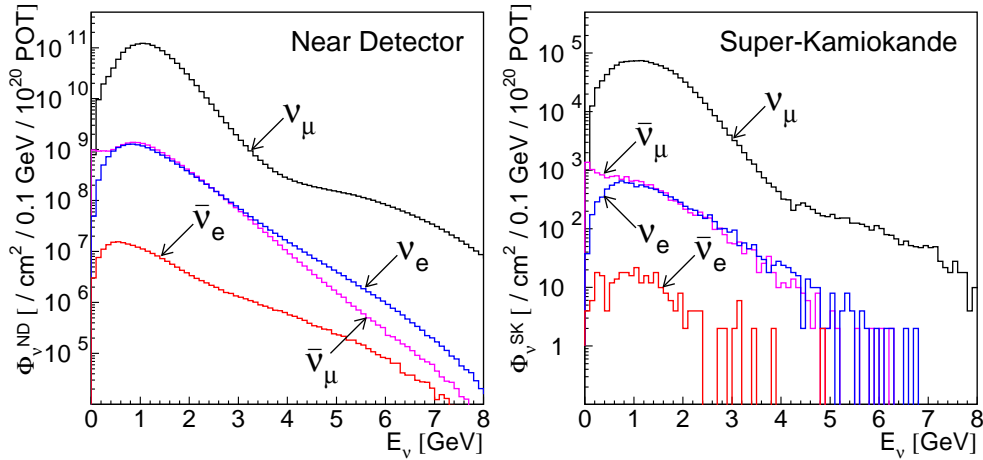


Figure 3. Simulated neutrino flux of K2K beam.

2.2. NuMI Beam

The NuMI beam [2] is located at the Fermi National Accelerator Laboratory in Illinois, USA, and it was initially constructed primarily for the MINOS experiment. In this section a description of NuMI as it was operated for the last 7 years is given first, before going on to discuss the upgrades for the NO ν A experiment that are underway at the time of writing. MINOS measured the NuMI flux at distances of 1 km and 735 km from the target and NO ν A will have the longest baseline of all such experiments at 810 km.

Protons from the Main Injector (MI) accelerator with a momentum of 120 GeV/c are used for the production of neutrinos and antineutrinos in the NuMI beamline. Typically, either 9 or 11 slip-stacked batches of protons from the MI are extracted in a single-shot onto the NuMI target giving neutrino pulses either 8 or 10 μ s long. Filling the MI with 8 GeV/c protons from the Booster accelerator takes about 0.7 s and then acceleration to 120 GeV/c takes a further 1.5 s, giving a total cycle time of about 2.2 s. A single-shot extraction from the MI contains around 3×10^{13} protons and the beam operated at a power of 300–350 kW over the last few years. By the time of the long-shutdown that started on 1st May 2012, NuMI had received nearly 16×10^{20} protons on target.

Figure 4 shows a schematic of the NuMI beamline and the components are described in sequence, starting on the far left with the protons coming from the MI. A water-cooled, segmented graphite target 2.0 interaction lengths long is used to produce the short-lived hadrons that give rise to the neutrinos. Two magnetic horns focus either positively or negatively charged particles towards a 675 m long decay volume, previously evacuated but now filled with helium. At the end of the decay volume a hadron absorber stops any remaining hadrons leaving just neutrinos and muons. Beyond that nearly 250 m of rock attenuates the muons leaving just the neutrinos.

The NuMI beamline was designed to be flexible in its operation with a number of parameters that could be adjusted to optimise the sensitivity to the physics topics of interest. The position of the target with respect to the first horn, the position of the second horn, the horn current and polarity could all be adjusted. The vast majority of data were taken in a “low energy” configuration that optimized the sensitivity to the atmospheric mass squared splitting by providing as large a flux as possible at the oscillation maximum for MINOS (around 1.4 GeV). This was achieved by inserting the target as far into the first horn as safely possible and having the second horn close to the first. A horn current of 185 kA was routinely used. Approximately 80% (20%) of the data were taken with the horn current polarity set to focus

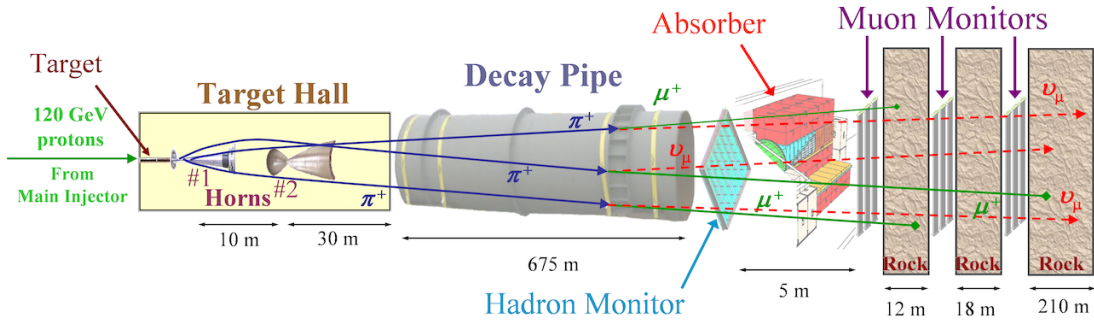


Figure 4. A schematic of the NuMI beamline. Protons from the Main Injector strike a graphite target, shown at the far left, and the resulting negatively or positively charged hadrons are focused by two magnetic horns. A 675 m long decay pipe gives the short-lived hadrons and muons time to decay. All hadrons remaining at the end of the decay volume are stopped by the absorber leaving just muons and neutrinos. The remaining muons are stopped by nearly 250 m of rock. Figure from [22].

positively (negatively) charged hadrons enhancing the production of neutrinos (antineutrinos). The energy spectrum measured by MINOS is shown in the results section in Figure 12.

The neutrino flavor composition of the on-axis NuMI beam is as follows: firstly, with the magnetic horn polarity set to focus positive hadrons a neutrino-enhanced beam is produced, giving rise to interactions in the (on-axis) MINOS near detector that are 91.7% ν_μ , 7.0% $\bar{\nu}_\mu$ and 1.3% $\nu_e + \bar{\nu}_e$; secondly, with the opposite polarity an antineutrino-enhanced beam is produced, giving near detector interactions that are 40% $\bar{\nu}_\mu$, 58% ν_μ , 2% $\nu_e + \bar{\nu}_e$ [23]. However, it should be noted that in the antineutrino-enhanced beam the $\bar{\nu}_\mu$ component comprises about 80% of the interactions below 6 GeV in the region where the oscillation effect is largest.

On a number of occasions and for relatively short periods the NuMI beamline was operated in non-standard configurations. These special runs were used to constrain uncertainties in analyses and better understand the beam. Examples include: runs with the horn current at 170 kA, 200 kA and 0 kA; and runs with the target pulled back out of the first horn by up to 2.5 m.

At the time of writing, the long accelerator shutdown to upgrade the NuMI beam for NO ν A is underway. With the shutdown of the Tevatron, two relatively straightforward changes will allow the NuMI beam power to be doubled to 700 kW. Previously the Recycler, a fixed field ring in the MI tunnel, was used to store antiprotons but now for NO ν A it will accumulate protons from the Booster while the MI is ramping. By parallelizing the accumulation and acceleration of protons for NuMI, and with a small increase in the MI ramp rate, the cycle time will be reduced from 2.2 s to 1.33 s. The second change is that the number of batches in the MI ring will be increased from 11 to 12 and the two that were previously used to produce antiprotons will now be used for NuMI.

In addition to the upgrades to the accelerator for NO ν A, modifications will also be made to the NuMI beamline. For the NO ν A detectors the position of the peak in the energy spectrum will be determined by the off-axis angle and so the flux will be optimized by focusing the maximum number of pions into the decay pipe with energies that allow a substantial fraction of them to decay within the 675 m long decay volume. The optimal configuration of the NuMI beamline for NO ν A will be to operate in a so-called “medium energy” configuration with the target sitting a meter or so back from the first horn and with the second horn positioned further downstream. This medium energy beam will have a peak energy of around 7 GeV for the on-axis experiments (e.g. MINOS+) compared to 1.9 GeV for NO ν A. The simulated energy spectrum

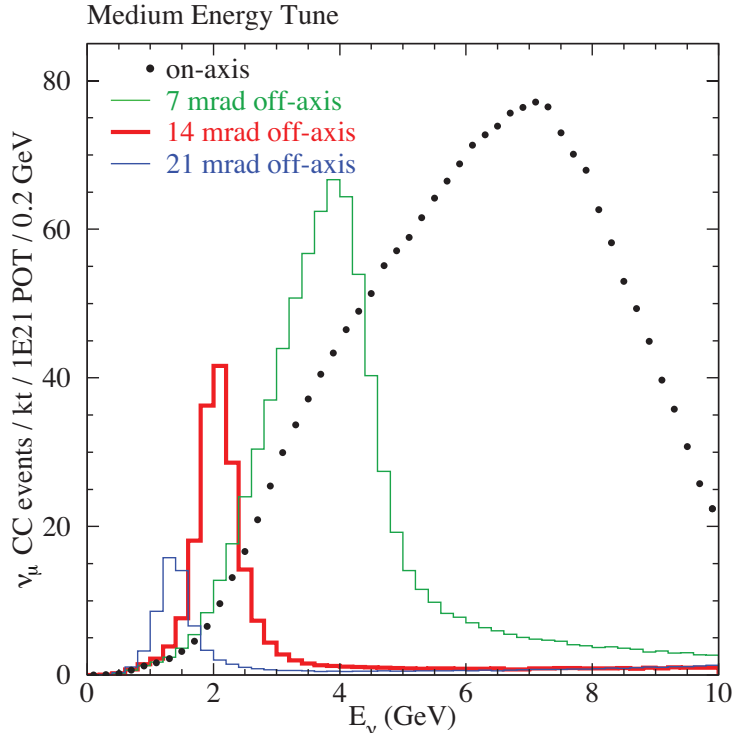


Figure 5. The simulated NuMI energy spectrum as it will be in the NO ν A-era with the beamline in the “medium energy” configuration. The NO ν A detectors will sit 14 mrad off-axis and the energy spectrum at that angle is shown by the red histogram. In contrast, the MINOS+ experiment will sit on-axis and so collect thousands of neutrino interactions per year that will be measured with an L/E resolution at the 10% level: the on-axis spectrum is shown by the black dots. The green and blue histograms further illustrate how the spectrum changes with the off-axis angle.

is shown in Figure 5. The NO ν A detectors, sitting 14 mrad off-axis, will see a beam flux with significantly higher purity than is obtained on-axis, having only about 1% $\bar{\nu}_\mu$ contamination of the ν_μ -enhanced beam and about 5% ν_μ contamination of the $\bar{\nu}_\mu$ -enhanced beam.

The target for the NO ν A era has been redesigned since there is no longer the constraint that it should be placed inside the first horn and increased reliability is expected. Beyond the upgrades underway for NO ν A, there is the possibility of increasing the beam power further; for example, the first phase of a proton driver could deliver 1.1 MW.

2.3. CNGS Beam

The CNGS beam [3, 24] is located at CERN on the border of Switzerland and France and the neutrinos are measured by experiments at the Gran Sasso Laboratory in Italy, 730 km away. CNGS uses 400 GeV/c protons from CERN’s SPS accelerator that are fast extracted in two 10.5 μ s spills 50 ms apart every 6 s. Each spill contains typically 2×10^{13} protons to give an average power of around 300 kW. The CNGS beam was commissioned in 2006 and the total exposure is expected to reach 1.9×10^{20} protons on target by the end of the 2012 run.

The CNGS target assembly consists of a magazine containing 5 separate targets, of which one is used at a time and the others are in-situ spares. Each target consists of a series of thirteen graphite rods 10 cm long, the first two are 5 cm in diameter and the remainder are 4 cm. The magnetic focusing system consists of a horn and a reflector that are pulsed at 150 kA

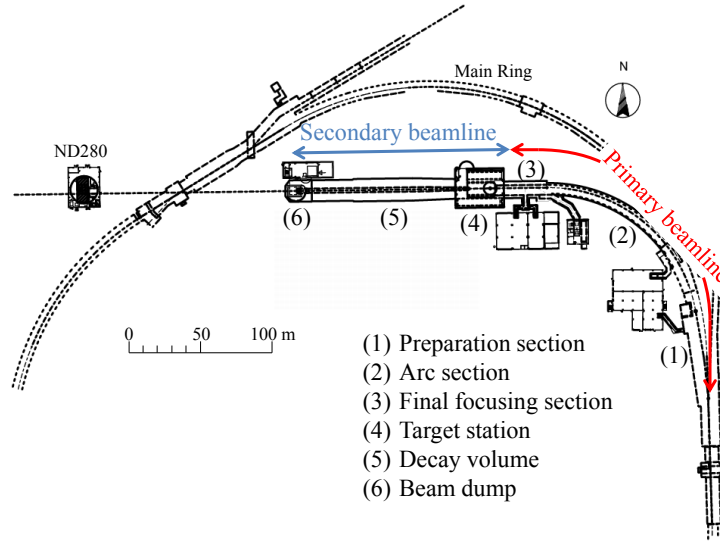


Figure 6. A schematic of the overall T2K beam facility, showing the primary and secondary beamlines plus the location of the ND280 detector complex.

and 180 kA respectively. An evacuated decay volume 1000 m long and 2.5 m in diameter allows the short-lived hadrons time to decay. At the end of the decay volume there is a graphite and iron hadron stop. Beyond that, two detector stations measure the remaining muons, which are used to derive the intensity and profile of the neutrino beam.

The CNGS beam is operated in a neutrino-enhanced mode and provides a high purity ν_μ source with $\bar{\nu}_\mu$ -contamination of 2% and $\nu_e + \bar{\nu}_e$ -contamination of less than 1%. The number of prompt ν_τ in the beam is negligible [25].

At the time of writing, no formal proposal for running the CNGS beam beyond the long LHC-shutdown in 2013 has been made by OPERA or other Gran Sasso experiments.

2.4. T2K Beam

The neutrino beam for the Tokai-to-Kamioka (T2K) experiment is produced at the Japan Proton Accelerator Research Complex (J-PARC) and measured by both near detectors locally and by Super-Kamiokande, 295 km from J-PARC. The T2K beam is an off-axis narrow band beam. Details of the experimental apparatus for T2K including the beamline are described in [4].

J-PARC is a high intensity proton accelerator complex located in Tokai village, Japan, whose construction was completed in 2009. The accelerator chain consists of a 181 MeV LINAC, 3 GeV Rapid Cycling Synchrotron and a 30 GeV Main Ring (MR). The design beam power of the MR is 750 kW. The proton beam used to produce the neutrino beam is extracted from MR in a single turn (fast extraction) with repetition cycle of 3.52 s at the beginning of operation in 2010 and 2.56 s now in 2012. The beam pulse of the single extraction consist of 8 bunches, 580 ns apart, making the pulse about 5 μ s long. The beam power achieved for stable operation as of summer 2012 was 200 kW which corresponds to 1.1×10^{14} protons/pulse (ppp) or 1.3×10^{13} protons/bunch (ppb).

The layout of the neutrino beam facility at J-PARC is illustrated in Figure 6. The extracted beam from MR is bent by about 90° to point in the Kamioka direction using 28 superconducting combined function magnets [26, 27, 28] and delivered to the production target.

The secondary beamline where the neutrinos are produced is shown in Figure 7. The production target is a 26 mm diameter and 90 cm long graphite rod, corresponding to

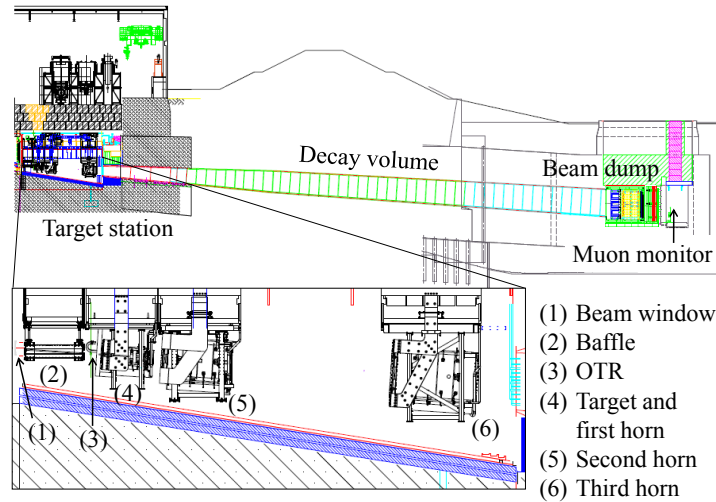


Figure 7. Schematic of T2K secondary beam line.

2 interaction lengths, in which about 80% of incoming protons interact. The secondary positive pions (and kaons) from the target are focused by three electromagnetic horns operated at a 250 kA pulsed current.

The target region is followed by a 110 m long decay volume filled with helium gas in which pions and kaons decay in flight into neutrinos. The beam dump, which consists of graphite blocks about 3.15 m thick followed by iron plates 2.5 m thick in total, is placed at the downstream end of the decay volume.

Muon monitors (MUMON) are placed just behind the beam dump to monitor the intensity and the profile of muons which pass through the beam dump on a spill-by-spill basis. High energy muons of > 5 GeV can penetrate the beam dump and reach the MUMONs.

The design principle of the J-PARC neutrino facility is that all parts which can never be replaced later, for example, the decay volume shielding and cooling pipes, beam dump cooling capacity, etc, are built such that they can be operated with up to 3 MW of beam power from the beginning. Parts that can be replaced are designed to be operated with a beam power up to 750 kW and have a safety factor of 2 to 3.

The neutrino beamline is designed so that the neutrino energy spectrum at Super-Kamiokande can be tuned by changing the off-axis angle down to a minimum of 2.0° from the current (maximum) angle of 2.5° . The unoscillated ν_μ energy spectrum at Super-Kamiokande with a 2.5° off-axis angle is shown in Figure 8.

The construction of the neutrino facility started in 2004 and was completed in 2009. Stable beam production for physics measurements started in January 2010 after careful commissioning. The Great East Japan Earthquake on March 11, 2011 damaged J-PARC and stopped the operation of the accelerators. After recovery work, the accelerator restarted operation in December 2011 and stable beam for T2K data taking was achieved in March 2012.

The J-PARC neutrino facility will provide an integrated number of protons on target of 7.5×10^{21} (equivalent to $750 \text{ kW} \times 5 \times 10^7 \text{ s}$), which is the approved exposure for T2K. With the present power upgrade scenario, this will take about 10 years.

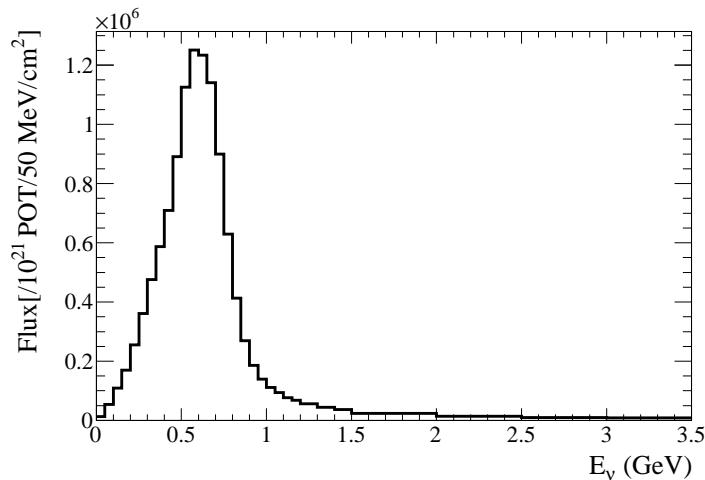


Figure 8. The unoscillated ν_μ flux at Super-Kamiokande with an off-axis angle of 2.5° and operation of the electromagnetic horns at 250 kA.

3. Detectors

In this section the detectors used by the experiments to achieve their diverse physics goals are described. Design of these detectors took into account multiple factors such as target mass, cost-effectiveness, particle flavor identification purity and efficiency, the beam energy spectrum and required baseline. The subsections below are time ordered and include K2K Near detectors and Super-Kamiokande (SK), MINOS, OPERA, ICARUS, the T2K ND280 complex and NO ν A.

3.1. K2K Near Detectors

The K2K Near detector complex was located at the KEK laboratory in Japan. The detectors were about 300 m from the beam-target, about 70 m of which was taken up with earth shielding. The detectors were designed to measure the flux and energy spectrum of the beam as it leaves KEK. Their mass composition was chosen to be primarily water so as to largely cancel common systematic uncertainties with Super-Kamiokande. These goals were achieved using a 1 kiloton water Čerenkov detector (the “1 kt”) and fine-grained detectors (FGD). A scintillating fiber detector (SciFi) [29], scintillating counters, a lead glass array (LG) and a muon range detector (MRD) [30] comprised the FGDs. For the second phase of K2K, the LG was replaced by the fully active scintillator-bar detector (SciBar) [31].

The 1 kt used the same technology as the Super-Kamiokande far detector with the same arrangement of photomultiplier tubes and the same 40% coverage. In total, 680 50 cm photomultiplier tubes were used to line an 8.6 m diameter, 8.6 m high cylinder.

The SciFi tracking detector used 20 layers of scintillating fibers, closely packed together in $2.6\text{ m} \times 2.6\text{ m}$ sheets that were separated by 9 cm. These layers were interleaved with 19 layers of water target contained in extruded aluminum boxes and read out using image-intensifier tubes and CCD cameras. The energy and angle of the muons produced in ν_μ CC interactions were measured using the MRD. This detector was designed to be big enough ($7.6\text{ m} \times 7.6\text{ m}$ in the plane transverse to the beam) to measure both the flux and the profile of the beam. The MRD consisted of 12 layers of iron absorber with vertical and horizontal drift tubes in between. The first 4 (upstream) layers were 10 cm thick and the remaining 8 layers were 20 cm thick. With 2.00 m of iron in total, up to 2.8 GeV/c muons could be stopped and their total energy measured.

The SciBar detector was an upgrade to the near detectors designed with the aim of improving

the measurement of CC quasi-elastic interactions and was installed in 2003. It was designed with the requirement of high purity and efficiency, with the suppression of inelastic CC interactions involving pions in the final state one of the main goals. The detector was “totally active” and could measure dE/dx for individual particles such as protons and pions. The SciBar detector consisted of 14,848 extruded scintillator strips (of dimension $1.3 \times 2.5 \times 300 \text{ cm}^3$) packed tightly together to make up the tracker part of the detector. On the downstream side of the tracker was an electromagnetic calorimeter, 11 radiation lengths thick and made of scintillating fibres & lead foils, called the Electron Catcher. This calorimeter was used to aid the measurement of electron showers and π^0 produced by neutrino interactions.

3.2. Super-Kamiokande Detector

The Super-Kamiokande detector [32] is the world’s largest land-based water Čerenkov detector with a total mass of 50 kilotonnes. SK is a 39 m diameter and 41 m high stainless steel cylindrical tank filled with ultra pure water that is located 1 km underneath Mt. Ikenoyama in Japan. The water tank is optically separated into a 33.8 m diameter and 36.2 m high cylindrically-shaped inner detector (ID) and outer detector (OD) by opaque black sheets and Tyvek sheets attached to a supporting structure. There are 11,129 inward-facing 50 cm diameter photomultiplier tubes (PMTs) lining the ID giving 40% coverage, and 1885 outward facing 20 cm diameter PMTs on the inner wall of the OD. The ID and OD are optically separated to allow interactions produced within the ID to be distinguished from those entering from outside (e.g. cosmic rays).

A key feature of SK is the ability to separate ν_μ CC events from ν_e CC by identifying the electron or muon. The muons, being heavier, produce sharper Čerenkov cones whereas electrons scatter more easily and the resulting “fuzzy” Čerenkov cone is effectively the sum of multiple overlapping cones all pointing in slightly different directions. The vertex for each interaction is reconstructed using the timing from all the hit PMTs and used to define the fiducial volume of 22.5 kilotonnes.

3.3. MINOS Detectors

The MINOS detectors [33] are magnetized tracking calorimeters made of steel and plastic scintillator optimized for measurements of muon neutrinos and antineutrinos with energies of a few-GeV. The Near Detector at Fermilab has a mass of 0.98 kilotonnes and the Far Detector at the Soudan Underground Laboratory in Minnesota, USA has a mass of 5.4 kilotonnes. The detectors have a planar geometry with the active medium comprised of solid plastic scintillator strips with neighboring planes having their strips orientated in perpendicular directions to give three dimensional tracking capability. The planes are hung vertically so as to be approximately perpendicular to the path of the beam neutrinos. In the detectors’ fiducial volumes 80% of the target mass is provided by steel planes and they are magnetized to provide average fields of 1.28 T and 1.42 T for the Near and Far detectors respectively. The steel planes are 2.54 cm thick (1.45 radiation lengths) and mounted on each one is, at most, a single 1.0 cm thick scintillator plane. Each scintillator plane comprises of up to 192 strips that are 4.1 cm wide and up to 8 m in length. There is an air gap between each plane of 2.4 cm in which the magnetic field is substantially smaller. A schematic of the Near and Far detectors is shown in Figure 9. The Far Detector planes are an 8 m wide octagonal shape and grouped together into two separately magnetized supermodules that are about 15 m in length. The Near Detector planes have a squashed octagon shape that is about 3 m wide and 2 m high. The Near Detector has two main parts: a fully instrumented region used for calorimetry and a muon spectrometer that is located downstream in the neutrino beam.

MINOS scintillator is made of polystyrene, doped with the fluors PPO (1%) and POPOP (0.03%), which is co-extruded with a thin 0.25 mm TiO_2 layer. A groove runs along the length of each strip into which a 1.2 mm wavelength-shifting (WLS) fibre optic cable is glued. On exiting

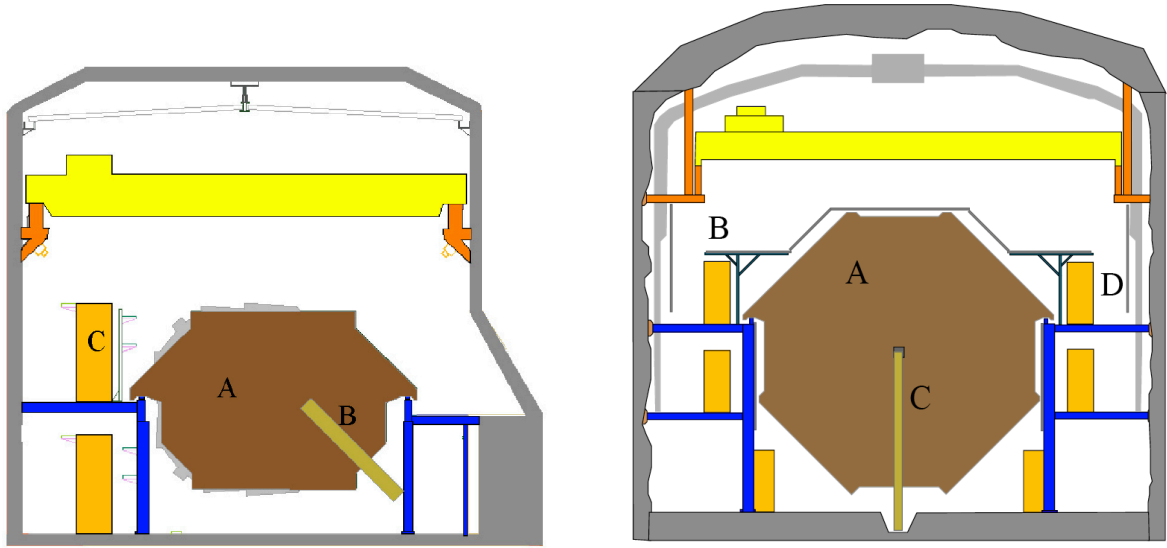


Figure 9. Schematics showing the end views of the MINOS Near (left) and Far (right) detectors. For the Near detector the label ‘A’ identifies the upstream steel plate, ‘B’ is the magnet coil and ‘C’ is an electronic rack. For the Far detector, ‘A’ identifies the steel plane at the end of the second supermodule, the furthest downstream in the beam, ‘B’ is the cosmic ray veto shield, ‘C’ is a magnet coil and ‘D’ is an electronics rack. The detectors are shown with different scales: the Near detector is 3 m wide compared to 8 m for the Far detector. Figure from [33].

the ends of the strips, the WLS fibers run together in a manifold to terminate in a connector. Clear fibre optic cables, with a longer 12 m attenuation length, are used to route the light to multi-anode photomultiplier tubes.

The Near and Far detectors were designed to be as similar as possible, although due to their different environments it was necessary to use different front-end electronics. On average, several neutrino interactions occur in the Near detector in every beam spill, whereas in the Far detector only a handful of neutrino interactions occur per day. The Near detector electronics digitizes the signal from each PMT pixel continuously during each beam spill at the frequency of the beam RF structure of 53.103 MHz. In contrast, the Far detector electronics has a dead time of at least $5 \mu\text{s}$ after each PMT dynode trigger. The Far detector self-triggers with high efficiency on neutrino interactions. In addition, the beam spill time is sent over the internet and used to record all detector activity in a $100 \mu\text{s}$ window around the beam spill. Both Near and Far detectors also record cosmic ray events, and at the Far detector, atmospheric neutrino events can be selected.

Neutrino energy reconstruction in MINOS involved both calorimetry of showers (although later analyses also used topological information to improve shower energy resolution) and either range or curvature of muon tracks. The calorimetric energy resolution of the MINOS detectors was determined to be $21.4\%/\sqrt{E} \oplus 4\%/E$ for electromagnetic showers and $56\%/\sqrt{E} \oplus 2\%$ for hadronic showers. The accuracy of the simulation of protons, pions, electrons and muons was determined using a specially constructed calibration detector that was exposed to CERN test-beams [34]. The test-beam data was also used to demonstrate that differences in the Near and Far detector readout systems could be corrected for by the calibration and the detector simulation [35] down to the 1% level.

In the Far detector the optimal fiducial volume of 4.2 kilotonnes included as many events as possible to reduce the statistical uncertainty on the oscillation parameters. Whereas in the Near

detector, with millions of events, the fiducial volume was optimized to make the best possible measurement of the neutrino energy spectrum and had a mass of 23.7 tonnes.

3.4. OPERA Detector

The OPERA detector is located 1400 m underground in Hall C at the Gran Sasso Laboratory, Italy and is optimized to enable a high purity selection of tau neutrino interactions on an individual event basis. A key signature of a ν_τ event is the topology of the tau decay. Substantial energy is carried away by the ν_τ produced in tau decay and due to the large tau mass the effect of missing transverse momentum often gives rise to a substantial change in direction (or “kink”) at the point along a track where the tau decays. With a mean lifetime of 0.29 picoseconds, corresponding to 87 μm at the speed of light, directly observing the tau in a necessarily massive detector is an experimental challenge.

The detector used by the OPERA collaboration is a hybrid consisting of a target constructed of fine grained emulsion and electronic detectors. Neutrino events are localized in the target using the scintillator target tracker (TT) detector and a spectrometer is used to measure the momentum and charge of muons. The target is divided into two supermodules with veto planes upstream. Each target region contains 75 000 emulsion cloud chambers (ECC), or “bricks”, which are constructed from 56 lead plates 1 mm thick that are interleaved with 57 nuclear emulsion films. Each ECC weighs 8.3 kg for a total target mass of around 1.25 kilotonnes. An automated system is used to extract the bricks identified by the TT from the detector. Scanning of the emulsion films is performed by automated microscopes located on the surface in Europe and Japan.

3.5. ICARUS Detector

The ICARUS T600 detector [36] is located in Hall B of the Gran Sasso Laboratory, Italy and consists of 760 tonnes of ultra-pure liquid argon (LAr) held at 89 K. The argon provides the target mass and the ionization medium for four time projection chambers (TPCs). These four TPCs come in two pairs, with each pair occupying a volume of $3.6 \times 3.9 \times 19.6 \text{ m}^3$. A shared cathode plane runs down the centre of each volume separating the two TPCs, giving a maximum drift path of 1.5 m. This detector provides exquisite electronic imaging of neutrino interactions in three dimensions with a position resolution of around 1 mm^3 over the whole detector active volume of about 170 m^3 .

An electric field of 500 V/cm is used to drift ionization electrons towards three parallel planes of wires arranged at 0° , $+60^\circ$ and -60° to the horizontal. These planes are situated along one side of each TPC and are separated by 3 mm. In total there are 53248 wires that have a pitch of 3 mm and lengths up to 9 m long. The first two planes (Induction-1 and Induction-2) provide signals in a non-destructive way before the charge is finally integrated on the Collection plane. Position information along the drift direction is provided by combining measurement of the absolute time of the ionising event with knowledge of the drift velocity (about 1.6 $\text{mm}/\mu\text{s}$ at the nominal electric field strength). VUV scintillation light from the liquid argon, measured by PMTs operating at cryogenic temperatures, provides the absolute timing information.

Electronegative impurities such as O_2 , CO_2 and H_2O were initially reduced by evacuating the detector for 3 months before filling and are generally maintained at below the 0.1 ppb level by recirculating the LAr through purification systems. Full volume recirculation can be accomplished in 6 days. A free electron lifetime of 1 ms corresponds to a 1.5 m drift distance and this has been successfully maintained for the vast majority of the time since the detector started operation in mid-2010.

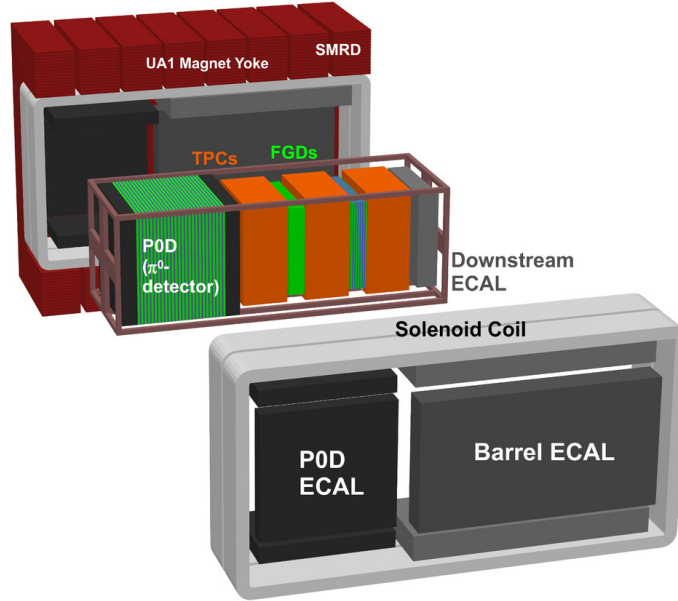


Figure 10. An exploded view of the ND280 off-axis near detector for the T2K experiment. The ND280 is a magnetized tracking detector comprising of several sub-detectors located inside the UA1 magnet (see the main body of text for detailed descriptions). Figure from [4].

3.6. T2K ND280 Detectors

The ND280 detector complex is located on the site of the J-PARC accelerator complex about 280 m downstream of the production target. The T2K experiment is formed of the ND280 detectors, the beamline and Super-Kamiokande. The ND280 detectors measure the neutrino energy spectrum and flavor content of the beam before it oscillates. Since the far detector is located 2.5° off-axis, the primary near detector is also located off-axis at the same angle. An on-axis near detector, INGRID, measures the neutrino beam profile and intensity.

The off-axis near detector is a magnetized tracking detector comprising of several sub-detectors located within the magnet recycled from the UA1 experiment at CERN. Figure 10 shows an exploded view of the off-axis ND280 detector displaying the π^0 detector (P0D), the tracker comprising of fine-grained detectors (FGDs) and time projection chambers (TPCs), the electromagnetic calorimeter (ECal), and side muon range detector (SMRD). The P0D consists of scintillating bars alternating with either a water target or brass or lead foil (to limit the range of any π^0 s). The FGDs consist of layers of finely segmented scintillator bars used to measure charged current interactions. These inner detectors are all surrounded by the ECal to catch any γ -rays that do not convert in the inner detectors. Finally, the SMRD sits in the return yoke of the magnet and measures the range of muons that exit the sides of the detector.

The on-axis INGRID detector consists of 14 identical modules arranged in a cross pattern with two groups: extending 10 m along the horizontal and vertical axes. A further two modules are located at off-axis positions a few meters above the horizontal and to each side of the vertical part of the cross. Each module is constructed from 9 steel plates 6.5 cm thick interleaved with 11 tracking scintillator planes. The planes consist of two sets of 24 scintillator bars measuring $1.0 \times 5.0 \times 120.3 \text{ cm}^3$, one set arranged to run vertically and the other horizontally. INGRID measures the center of the beam to a precision of 10 cm, equivalent to 0.4 mrad.

3.7. $NO\nu A$ Detectors

The $NO\nu A$ [15] far detector will be located 14 m off the NuMI beam axis, 810 km from the NuMI target, off the Ash River Trail in northern Minnesota, USA. The Ash River Trail is the most northern road in the United States near the NuMI beam line. The $NO\nu A$ near detector will be located on the Fermilab site about 1 km from the NuMI target, also at an angle of 14 m to NuMI beam.

The $NO\nu A$ detectors can be described as totally active, tracking, liquid scintillator calorimeters. The basic cell of the far detector is a column or row of liquid scintillator with approximate transverse dimensions 4 cm by 15.6 m and longitudinal dimension 6 cm encased in a highly-reflective polyvinyl chloride (PVC) container. A module of 32 cells is constructed from two 16-cell PVC extrusions glued together and fitted with appropriate end pieces. Twelve modules make up a plane, and the planes alternate in having their long dimension horizontal and vertical. The far detector will consist of a minimum of 928 planes, corresponding to a mass of approximately 14 kt. Additional planes are possible depending on available funds at the end of the project. Each plane corresponds to 0.15 radiation lengths.

The $NO\nu A$ near detector will be identical to the far detector except that it will be smaller, 3 modules high by 3 modules wide, with 192 planes. Behind the near detector proper will be a muon ranger, a sandwich of 10 10-cm iron plates each followed by two planes of liquid scintillator detectors. $NO\nu A$ has also constructed a near detector prototype called the NDOS (Near Detector On the Surface) which has been running since November 2010 on the surface at Fermilab, off axis to both the NuMI and Booster neutrino beams. Figure 11 contains a drawing of the $NO\nu A$ detectors.

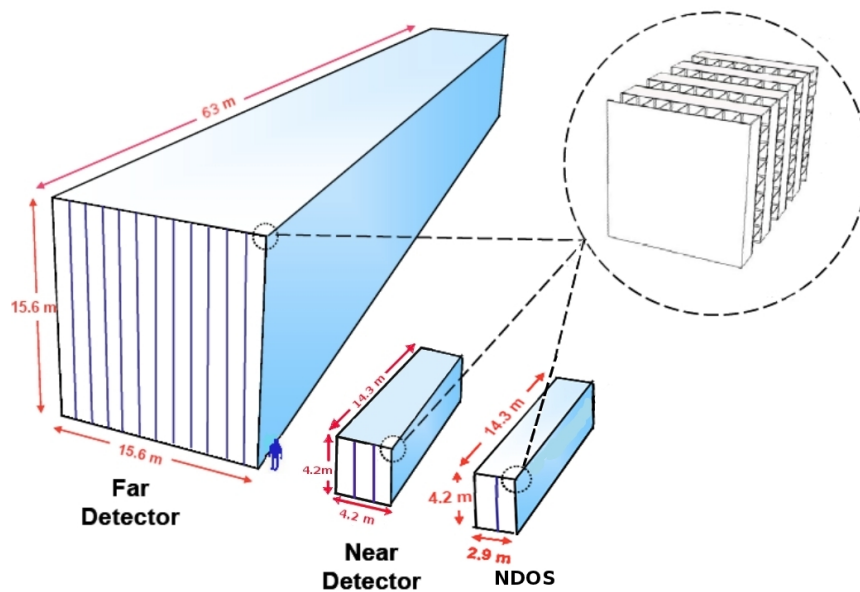


Figure 11. Drawings of the $NO\nu A$ far and near detectors. The human figure at the base of the far detector is for scale.

Light is extracted from each liquid scintillator cell by a U-shaped 0.7-mm wavelength-shifting fiber, the ends of which terminate on a pixel of a 32-pixel avalanche photodiode (APD), which is mounted on the module. The APD is custom-made for the $NO\nu A$ experiment by the Hamamatsu Corporation to optimize the match to the two fiber ends per pixel. Light from the far end of the cell is preferentially attenuated at the lower wavelengths, so that the peak of the spectrum is at about 540 nm. The use of APDs is crucial for the experiment since they have a quantum

efficiency of approximately 85% at this wavelength compared to 10% for a photomultiplier with a bialkali photocathode. The system is designed to produce a minimum of 20 photoelectrons from the far end of the cell for the passage of a minimum ionizing particle at normal incidence. The APD is run at a gain of 100, so low noise is required for efficient operation. The APD is cooled to -15°C by a thermoelectric cooler to reduce the thermal noise of the APD to an acceptable limit.

The NO ν A front-end electronics runs in continuous digitization mode at 2 MHz for the far detector and 8 MHz for the near detector. It delivers GPS time-stamped, pedestal subtracted, and zero-suppressed data to the data acquisition system (DAQ). At the far detector, the DAQ buffers the data for up to 20 seconds while awaiting a beam spill time message from Fermilab via Internet. All data within a 30 μs window around the 10 μs beam spill will be recorded for offline analysis.

4. Results on $\nu_\mu \rightarrow \nu_\tau$: the dominant oscillation mode

The dominant oscillation mode for all long-baseline accelerator experiments performed to date is $\nu_\mu \rightarrow \nu_\tau$. This channel was used by K2K [37, 5] and MINOS [38] to provide essential confirmation of the neutrino oscillations observed by Super-Kamiokande in atmospheric neutrinos [11]. Accelerator experiments with their fixed baselines, L , and high energy resolution detectors allow precise measurement of L/E . In turn, this allows resolution of the oscillatory quantum-mechanical interference pattern and precise measurements of $|\Delta m^2|$ and $\sin^2(2\theta)$: these results are described here in section 4.1. The corresponding measurements for muon antineutrinos are described in section 4.2.

Direct observation of tau appearance by OPERA will further confirm $\nu_\mu \rightarrow \nu_\tau$ as the dominant mode of oscillation and the results from the first half of their data set [25, 39] are described in section 4.3.

4.1. Precision measurement of $|\Delta m^2|$ and $\sin^2(2\theta)$

In an accelerator experiment, measurement of $|\Delta m^2|$ and $\sin^2(2\theta)$ is performed by observing the energy dependent disappearance of muon neutrinos. The fixed baselines, L , are known to high precision and so contribute a negligible uncertainty to measurement of L/E , which is dominated by the energy resolution of the detectors. The energy at which the maximum disappearance occurs is a measure of $|\Delta m^2|$ and the disappearance probability at that point is given by $\sin^2(2\theta)$. Figure 12 shows the energy spectrum of muon neutrino candidate events in the MINOS far detector where the energy dependent deficit can be clearly seen, with the maximum disappearance occurring at around 1.4 GeV for the 735 km baseline.

A crucial ingredient to enabling precise measurements of the oscillation parameters is event-by-event identification of whether the observed interactions are neutral-current (NC) or charged-current (CC) events. In the absence of sterile neutrinos, the spectrum of NC events is unchanged due to oscillations and has to be separated from the muon neutrino CC sample. For the experiments performed to date, identification of the flavor of CC events has been of secondary importance to the separation of NC events since the vast majority of CC events are muon flavor. Given the tau production threshold at a neutrino energy of around 3.5 GeV, this appearance mode is naturally suppressed in K2K, MINOS, T2K and NO ν A due to their lower beam energies and so relatively few ν_τ CC interactions occur. The appearance of electron neutrinos is a subdominant effect (detailed in section 5) that contributes, for example, only around 1% of the event rate in MINOS. The performance of the different experiments in selecting a ν_μ CC event sample is discussed below.

4.1.1. K2K ν_μ Disappearance Results

K2K was the first accelerator long-baseline experiment, taking data from 1999–2004. The

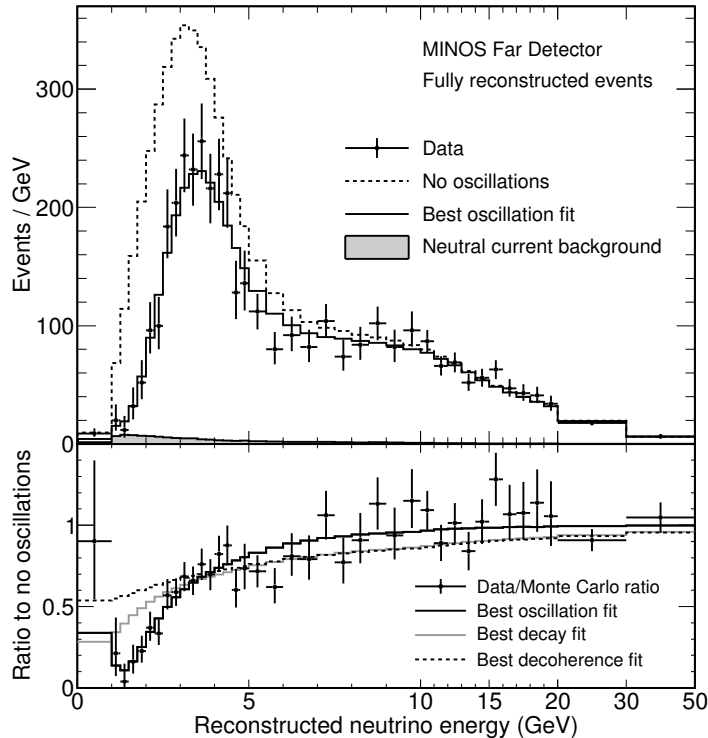


Figure 12. The energy spectrum of fully reconstructed muon neutrino candidate events in the MINOS Far detector (top pane). Both the no oscillation hypothesis and the best oscillation fit are shown. The shaded region shows the expected neutral-current background. The ratio to no oscillations (bottom pane) displays the best fits to models of neutrino decay and neutrino decoherence, where they are seen to be disfavored at high significance (7σ and 9σ respectively).

neutrino beam was produced and measured at KEK in Japan and then observed 250 km away at the Super-Kamiokande detector. K2K saw 112 beam-originated events in the fiducial volume of Super-Kamiokande with an expectation of $158.1^{+9.2}_{-8.6}$ without oscillation [5]. The water Čerenkov detector allowed separation of 58 single-ring muon-like events in which a distortion of the energy spectrum was seen. At the K2K beam energy these muon-like events contained a high fraction of quasi-elastic events and the incoming neutrino energy was reconstructed using two-body kinematics. Combining information from both the shape of the energy spectrum and the normalization, K2K determined that the probability of obtaining their data in the case of null-oscillations was 0.0015% (4.3σ) thus confirming the Super-Kamiokande atmospheric neutrino results. The K2K 90% C.L. allowed region in the $|\Delta m^2| - \sin^2(2\theta)$ plane is shown by the magenta line in Figure 13.

4.1.2. MINOS ν_μ Disappearance Results

MINOS started data taking in 2005 and ran for 7 years through April 2012. Around 80% of the data was taken with the beam optimized to produce neutrinos and the remaining 20% antineutrinos (see section 4.2 for a description of the $\bar{\nu}_\mu$ disappearance results). The first ν_μ disappearance results from MINOS are given in [38] and detailed in a longer paper [43]. Updated results are given in [44] and those presented here are taken from [40]. Additionally, the results from the preliminary analysis using the full MINOS data set [45] are also summarised here.

The geometry of the MINOS detectors allows three dimensional reconstruction of tracks

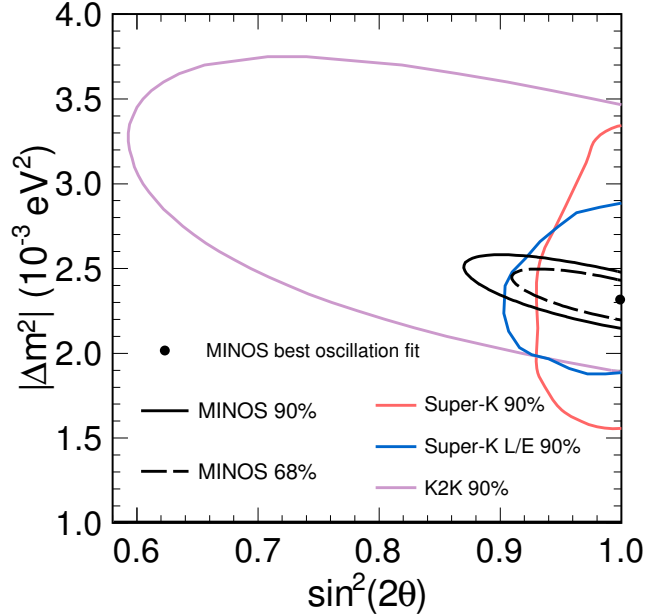


Figure 13. The 90% confidence regions for $|\Delta m^2|$ and $\sin^2(2\theta)$. Results shown are published contours from K2K [5], MINOS [40] and Super-Kamiokande [41, 42]. For the latest but still preliminary results see Figure 14.

and showers. Using the reconstructed vertex information a fiducial volume cut was made that separated incomplete and partially reconstructed events occurring at the edge of the detector from those that were fully reconstructed. As mentioned above, a crucial step in this analysis was the separation of ν_μ CC events from NC events. For the first results a particle identification parameter was constructed using probability density functions for the event length, the fraction of the energy contained in the track, and the average pulse height per plane. The later results used an improved technique based on a k-nearest-neighbor algorithm (kNN). This kNN technique used the energy deposition along a track and its fluctuation to discriminate muons from spurious tracks reconstructed from hadronic activity in NC interactions. For the most recent analysis an overall efficiency for selecting ν_μ CC events of 90% was achieved. The first results made a selection on the charge-sign of the muon but later analyses have included the 7% antineutrino component of the neutrino-enhanced beam, which had a significantly higher average energy [46].

Near detector data was used to substantially reduce systematic effects on this measurement that would otherwise arise from limited knowledge of the neutrino flux and cross-sections. Both the Near and Far Detectors measured a product of flux times cross-section and by doing a relative measurement, the uncertainties on that product canceled to first order. However, the flux was not the same at the Near and Far detectors: one saw a line-source of neutrinos and the other saw what was effectively a point source. The Far Detector flux was populated by neutrinos from more forward decaying pions and so the spectrum was somewhat harder than at the Near detector. The beamline simulation incorporated and was used to estimate these largely geometrical effects.

Due primarily to the flux and cross-section uncertainties, the Near detector data differed from the simulation by up to 20% as a function of energy. An extrapolation procedure used

the Near Detector measurements to predict the Far Detector energy spectrum via a number of steps as follows: subtracting the estimated background from the Near Detector energy spectrum; deconvolving the effects of Near detector energy resolution; using a transfer matrix to account for the different flux at the Far Detector; weighting each energy bin according to the oscillation probability; reintroducing the effect of energy resolution at the Far Detector; and adding in the estimated Far Detector background. With all these steps complete an oscillated Far Detector prediction was obtained for comparison with the data.

Several sources of systematic uncertainty were accounted for in this measurement. The three largest uncertainties on the measurement of $|\Delta m^2|$ were on the absolute energy scale of hadronic showers, the absolute energy scale of muons and the relative normalization of event rates between Near and Far Detectors. Other uncertainties included NC contamination, the relative hadronic energy scale, cross-sections and beam flux. Overall, the statistical error on the MINOS measurement of $|\Delta m^2|$ was still more significant than the systematic uncertainty.

The largest three systematic uncertainties on the measurement of $\sin^2(2\theta)$ were on the NC contamination, cross-sections, and the relative hadronic energy scale. However, the MINOS measurement of $\sin^2(2\theta)$ was dominated by the statistical uncertainty, with the systematic uncertainty being smaller by more than a factor of four.

Every NuMI beam event with a reconstructed muon was included in the likelihood fit to extract the oscillation parameters. These events were split into 7 event categories to extract the maximum information. Partially reconstructed events, where the neutrino interacted in the rock outside the detector or in the outer edges of the detector, were a separate category and only their reconstructed muon information was used (any shower energy was ignored due to its limited use for this sample). Fully reconstructed ν_μ CC candidate events were separated by the charge-sign of the muon. Positively charged events formed their own single sample but the negatively charged events were divided into 5 categories using their estimated energy resolution (for example, a highly-elastic CC event where most of the neutrino energy was carried away by the muon was measured more precisely than an inelastic event where shower energy fluctuations smeared the measurement). The four dominant systematic uncertainties were included as nuisance parameters and the mixing angle was constrained by the physical boundary at $\sin^2(2\theta) = 1$.

Thousands of beam neutrino interactions have been recorded at the MINOS Far detector and used, as described above, to make the world's most precise measurement of $|\Delta m^2| = (2.32^{+0.12}_{-0.08}) \times 10^{-3} \text{ eV}^2$ while constraining $\sin^2(2\theta) < 0.90$ at 90% C.L. [40]. Figure 12 shows the fully reconstructed events recorded by MINOS where the distortion of the energy spectrum expected by oscillations can be seen and contrasts with that expected from alternative models of neutrino disappearance such as neutrino decay or decoherence (they are excluded at 7 and 9 σ respectively). The MINOS contours associated with this published result are shown in Figure 13 (updated but preliminary results from MINOS are shown in Figure 14).

Recently, preliminary MINOS results using the complete data set have been released [45]. The total neutrino-enhanced beam exposure is 10.7×10^{20} POT, 50% more than the previous result given above. Furthermore, two additional data sets are included: firstly, the antineutrino-enhanced beam data (3.36×10^{20} POT); and secondly, atmospheric neutrinos and antineutrinos (37.9 kiloton-years). While still well within the previous 1σ contours, the best fit point for this new analysis has moved slightly away from maximal mixing to $|\Delta m^2| = (2.39^{+0.09}_{-0.10}) \times 10^{-3} \text{ eV}^2$ and $\sin^2(2\theta) = 0.96^{+0.04}_{-0.04}$ (the shift in upwards in $|\Delta m^2|$ being correlated with the shift downward in $\sin^2(2\theta)$, due to the required overall normalization being similar to the previous result).

The MINOS preliminary 90% C.L. allowed region in the $|\Delta m^2| - \sin^2(2\theta)$ plane is shown in Figure 14 by the solid black contour. The latest results from Super-Kamiokande [47] (preliminary) and T2K [48] are shown alongside for comparison. All the results presented here

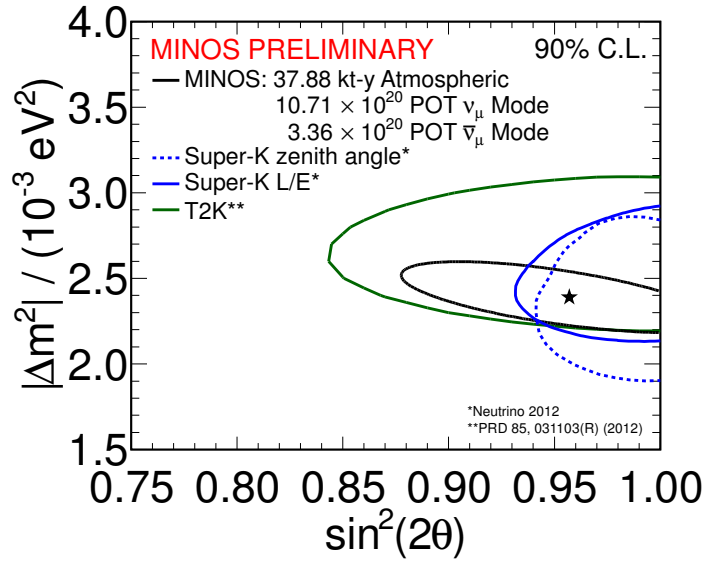


Figure 14. Preliminary 90% confidence regions for $|\Delta m^2|$ and $\sin^2(2\theta)$ (except for T2K, which is published). Results are shown for MINOS [45], T2K [48] and Super-Kamiokande [47]. The MINOS results shown here are a combination of NuMI beam data and atmospheric neutrino data.

use the 2-flavor approximation.

4.1.3. T2K ν_μ Disappearance Results

T2K started taking data in 2010 and was the first experiment to use an off-axis beam to observe muon neutrino disappearance [48]. The exposure for the first result was 1.43×10^{20} POT and is expected to increase substantially over the next few years. In the Super-Kamiokande far detector, 31 fully-contained muon-like ring events were observed against an expectation of $104 \pm 14(\text{syst})$ without neutrino oscillations. The observed neutrino energy spectrum alongside the predicted spectra with and without oscillation are shown in Figure 15.

The values of the oscillation parameters obtained are consistent with both MINOS results and Super-Kamiokande atmospheric neutrinos. Interestingly, the T2K constraints on $\sin^2(2\theta)$ already approach the limit set by MINOS. This demonstrates the sensitivity of T2K where the energy peak of the narrow band, off-axis, beam is positioned close to the oscillation maximum and consequently a large fraction of the ν_μ flux disappears. The T2K contours are shown in Figure 14 alongside the latest MINOS results.

4.2. Measurements of $|\Delta \bar{m}_{\text{atm}}^2|$ and $\sin^2(2\bar{\theta})$

MINOS accumulated 20% of its total exposure with the NuMI beam configured to enhance production of antineutrinos and made the first direct measurement of muon antineutrino disappearance [49]. The CPT theorem, that provides the foundation of the standard model, predicts identical disappearance of neutrinos and antineutrinos in vacuum and the measurements described here allow precision tests of that hypothesis as well as other models of new physics. The first antineutrino result from MINOS reported tension with the neutrino results but with further data the results are now consistent [50, 45]. In addition to these results, the 7% antineutrino component of the neutrino-enhanced beam has also been analyzed [46]; these data provided a higher statistics sample of $\bar{\nu}_\mu$ events in the 5–15 GeV range, allowing the oscillation probability

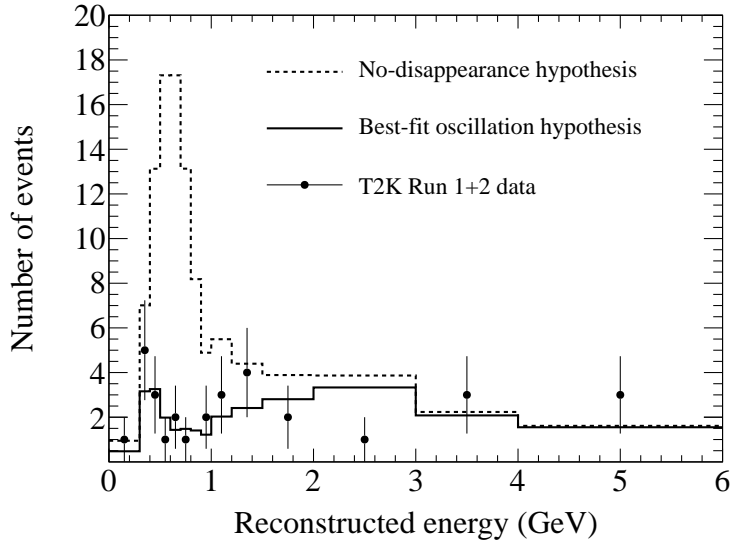


Figure 15. Reconstructed neutrino energy spectra of T2K ν_μ disappearance analysis.

to be measured with greater precision in that region. The MINOS magnetized detectors were essential to obtaining a high purity sample of $\bar{\nu}_\mu$ CC events and making the measurements reviewed here.

The antineutrino-enhanced beam flavor composition, described in section 2, was 40% $\bar{\nu}_\mu$, 58% ν_μ , 2% $\nu_e + \bar{\nu}_e$ [23]. The reason for the large number of neutrinos was two-fold: firstly, the antineutrino cross-section is about 2–3 times lower than for neutrinos; and secondly, the yield of negative pions from the beam target was lower than for positive pions. However, the ratio of antineutrinos to neutrinos in the NuMI beam varied strongly as a function of energy and below 6 GeV about 80% of the interactions were antineutrinos (and that’s where the oscillation effect was largest for MINOS). Discrimination of muon neutrinos from antineutrinos was performed on an event-by-event basis by analyzing the track curvature in the detector’s magnetic field. Efficiency and purity was estimated from the MC simulation at 91.6% and 99.0% respectively for the Far Detector.

With the magnetized detectors able to cleanly separate positive and negative muons, the rejection of NC events was an important requirement for this analysis. The k-nearest-neighbor multivariate technique used for the neutrino analysis (see section 4.1) was used to separate $\bar{\nu}_\mu$ CC events from NC. The procedure for extrapolating Near Detector antineutrino data to make a Far Detector prediction was essentially the same as for the neutrino analysis. The detector and beamline simulations were reperformed for antineutrinos to calculate, for example, the required detector resolution deconvolution matrix and flux transfer matrix for $\bar{\nu}_\mu$. A slight modification to the oscillation step of the extrapolation was required to allow neutrinos and antineutrinos to oscillate differently in the simulation.

Systematic uncertainties on the measurement of the antineutrino oscillation parameters were similar to those described for neutrinos in section 4.1.2 above. An additional uncertainty was included on the level of neutrino contamination and the knowledge of the neutrino oscillation parameters. The MINOS measurement of neutrino parameters is not yet systematically limited and given both the factor of 3 lower exposure recorded for antineutrinos (3.36×10^{20} POT) and the reduced number of $\bar{\nu}_\mu$ per POT, the antineutrino measurement is dominated by statistical uncertainties.

Recently, a preliminary version of the MINOS measurements of antineutrino oscillation parameters using the full data set have been released [45]. This analysis incorporates three

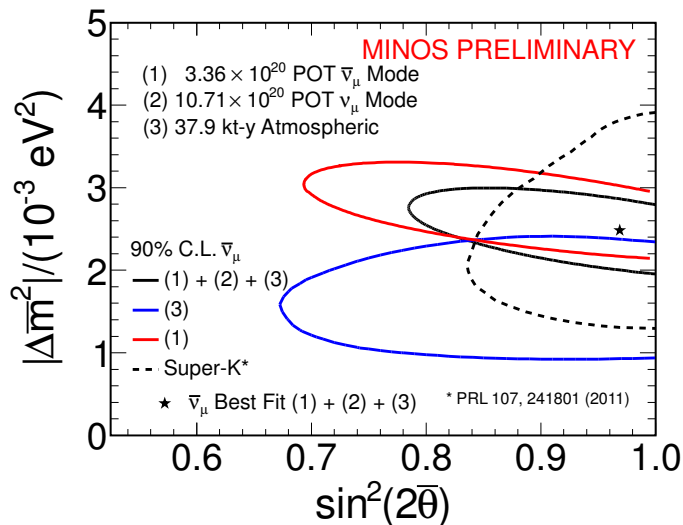


Figure 16. The 90% confidence regions for antineutrino parameters $|\Delta\bar{m}_{\text{atm}}^2|$ and $\sin^2(2\bar{\theta})$. Antineutrino results are shown from Super-Kamiokande [51] (dashed black) alongside the latest preliminary results from MINOS [45] (solid black). The MINOS results used three data sets: (1) atmospheric antineutrinos; (2) antineutrinos from the NuMI beam operating in antineutrino-enhanced mode; and (3) antineutrinos from the neutrino-enhanced beam. The red contour shows the result from just the NuMI beam data and the blue contour from just the atmospheric antineutrino data.

distinct data sets: the antineutrino-enhanced NuMI beam data (3.36×10^{20} POT); the antineutrinos in the neutrino-enhanced beam (10.7×10^{20} POT); and atmospheric antineutrino data (37.9 kiloton-years). The antineutrino mass splitting was measured to be $|\Delta\bar{m}_{\text{atm}}^2| = (2.48_{-0.27}^{+0.22}) \times 10^{-3} \text{ eV}^2$ and the mixing angle $\sin^2(2\bar{\theta}) = 0.97_{-0.08}^{+0.03}$ with $\sin^2(2\bar{\theta}) > 0.83$ at 90% C.L. The antineutrino contour from MINOS is shown in Figure 16 by the solid black line. Also shown for comparison is the result from the Super-Kamiokande measurement (dashed black) of the combined flux of atmospheric muon neutrinos and antineutrinos [51]. The red contour shows the result from just the NuMI beam data and the blue contour from just the MINOS atmospheric antineutrino data. The MINOS measurements provide the highest precision on the antineutrino mass squared splitting while Super-Kamiokande measures the antineutrino mixing angle most precisely.

The uncertainty on the difference in the atmospheric mass squared splittings of neutrinos and antineutrinos is currently dominated by the statistical precision on the antineutrino measurements, by about a factor of 2–3. In the future, NO ν A will improve measurement of all the disappearance related parameters for neutrinos and antineutrinos. Importantly for future precision tests of CPT symmetry, several systematic errors on the difference between $|\Delta m^2|$ and $|\Delta\bar{m}_{\text{atm}}^2|$ will be significantly smaller than the systematic uncertainty on the two absolute measurements taken separately.

4.3. Searches for ν_τ Appearance

The observation of ν_τ appearance with a ν_μ source would directly confirm the hypothesis of $\nu_\mu \rightarrow \nu_\tau$ oscillations as the cause of the disappearance affect observed by atmospheric and accelerator experiments. This is the goal of the OPERA experiment [7]. Furthermore, there is currently no observation at the 5-sigma level of the appearance of neutrino flavors due to

oscillations, only disappearance. The next few years should see the conclusive observation of both ν_τ appearance with OPERA and ν_e appearance with T2K and NO ν A, demonstrating key aspects of the 3-flavour neutrino oscillation model.

The kinematic threshold for τ production from ν_τ interactions is around 3.5 GeV and at that energy the first maximum of the oscillation probability occurs at a baseline of approximately 2500 km. For a fixed baseline, matching the energy of the beam with the peak of the product of ν_τ cross-section times oscillation probability maximizes the number of ν_τ interactions in the detector for a given integrated flux: this is largely what the OPERA experiment has done with the CNGS beam. As described in section 2, the experiments using the CNGS and NuMI beams have very similar baselines, 730 km vs. 735 km respectively, but differ substantially in their average neutrino energies of 17 GeV and 3 GeV respectively due to the different physics goals of the experiments.

The OPERA experiment at LNGS started taking data in 2008 with the CNGS beam [3, 24] and in 2010 they published the observation of their first ν_τ candidate event [25]. As described in section 3, the OPERA detector consists of lead-emulsion bricks with electronic detectors to pinpoint the bricks in which neutrino interactions occurred.

The first candidate ν_τ event observed by OPERA is shown in Figure 17. A detailed description of the likely candidates for each of the numbered tracks is given in [25]. This event is compatible with the decay $\tau^- \rightarrow \rho^- \nu_\tau$ with the $\rho(770)$ decaying to a π^0 and π^- .

A preliminary analysis of further data has recently been released and a second ν_τ candidate has been observed [52]. This event was seen in the 2010-11 data set and it satisfies the selection criteria for $\nu_\tau \rightarrow 3$ hadrons. In the data set analyzed to date, the preliminary background estimate was 0.2 events and 2.1 signal events were expected. The Poisson probability of observing 2 or more events given a background expectation of 0.2 is 1.75%.

Atmospheric neutrino experiments have a relatively large number of ν_τ events in their data samples, given the broad range of available energies and the Earth's 13,000 km diameter. Super-Kamiokande has published 2.4σ evidence for ν_τ appearance [53] using candidate events selected for the expected shape of ν_τ interactions and characteristics of τ leptons. This statistical separation is a complementary approach to OPERA's goal of directly observing individual ν_τ events. At the time of writing a new SK result was published on the arXiv that provides evidence for ν_τ appearance at the 3.8σ confidence level [54]. In the future, MINOS+ will also have a relatively large number of ν_τ events (around 90/year with the ν_μ -enhanced beam) and with sufficient rejection of backgrounds will have sensitivity to this oscillation channel [19].

5. Results on $\nu_\mu \rightarrow \nu_e$: the sub-dominant oscillation mode

With the baselines and neutrino energies (the L/E) used by the experiments described in this review, $\nu_\mu \rightarrow \nu_e$ is a sub-dominant oscillation mode (although at an L/E 25 times larger, the solar mass splitting would have a significant effect and ν_e 's would then make up the majority of the flux).

Measurements of the sub-dominant $\nu_\mu \rightarrow \nu_e$ oscillation mode are of great importance for a number of reasons: firstly, its discovery will demonstrate the full 3-flavor neutrino oscillation model; secondly, with a non-zero value of θ_{13} a door is opened to discovering CP violation in the lepton sector; and thirdly, by exploiting the neutrino-matter interaction that the neutrinos and antineutrinos experience as they propagate through the Earth, the neutrino mass hierarchy (the sign of Δm_{32}^2) can also be determined.

Measurements of the sub-dominant mode made using accelerator neutrino beams are highly complementary to those made using nuclear reactors. The reactor neutrino experiments Double Chooz [16], Daya Bay [18] and RENO [18] have recently observed sub-dominant neutrino oscillations via the disappearance of $\bar{\nu}_e$ over a distance of around 1.5 km. This channel is only sensitive to θ_{13} and so a direct measurement can be made. In contrast, the accelerator

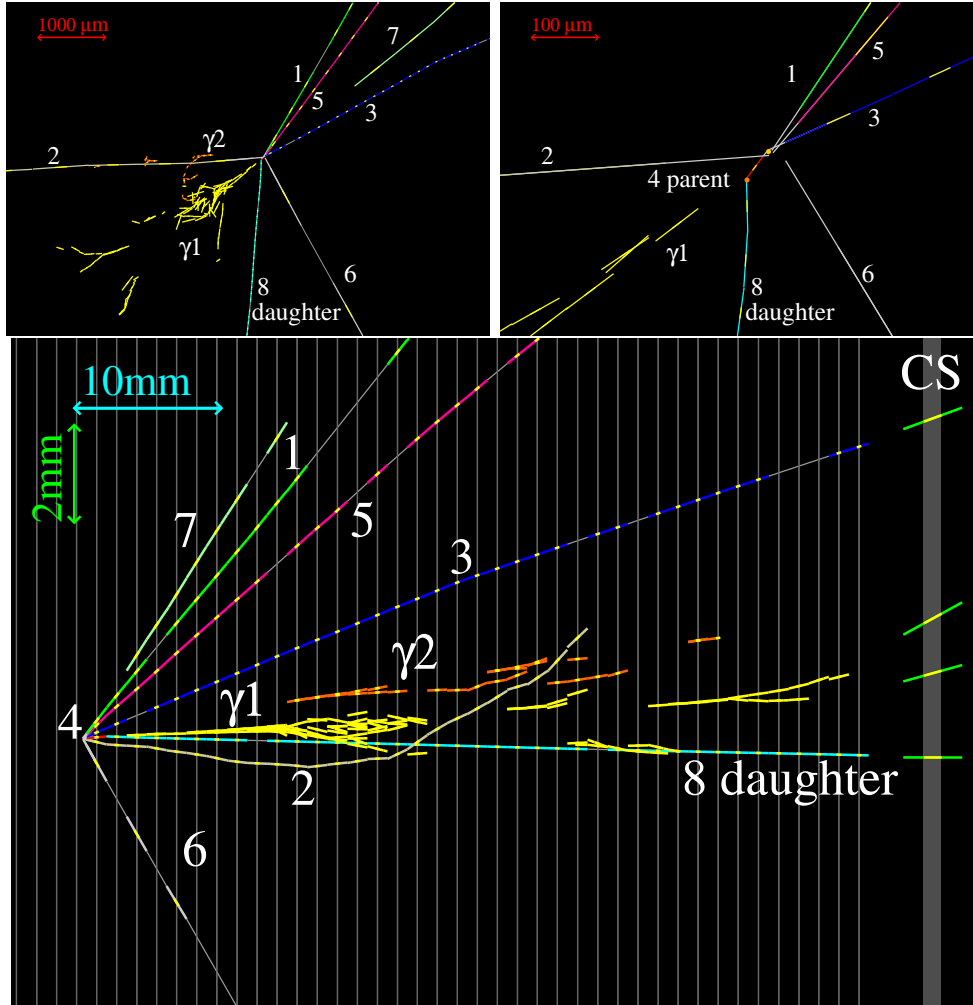


Figure 17. The first candidate ν_τ event observed by the OPERA experiment. The top plots show the transverse view with the right plot being a zoom of the left. The bottom plot shows the longitudinal view. The short red track (labeled as “4 parent”) is identified as being due to the τ lepton and the track of what is thought to be the tau-daughter is shown in turquoise (labeled as “8 daughter”). A kink is clearly seen, particularly in the zoomed transverse view (top right), and demarked by the change in color from red to turquoise along the track. A detailed description of the likely candidates for each of the numbered tracks is given in the OPERA paper [25].

experiments are sensitive to θ_{13} , the CP phase, the mass hierarchy and the octant of θ_{23} , enabling a rich set of measurements to be made using a combination of different baselines and energies with neutrinos and/or antineutrinos.

In this section the electron neutrino appearance results from K2K, MINOS and T2K are presented. A key feature of these experiments is their ability to distinguish the rare occurrence of electron flavor neutrino interactions from among the many more ν_μ CC events and NC events from all neutrino flavors. For example, electron neutrino events in MINOS contribute only around 1% of the event rate. The significant majority of ν_μ CC events are relatively easy to reject due to the presence of the muon. However, in highly inelastic ν_μ CC events the muon can escape detection and should the hadronic shower have a significant electromagnetic component (from, for example, $\pi^0 \rightarrow \gamma\gamma$) then it can be misidentified as an electron neutrino event.

5.1. K2K ν_e Appearance Results

The first long-baseline accelerator neutrino experiment to search for electron neutrino appearance was K2K [55, 56]. This measurement exploited the ability of the Super-Kamiokande detector to distinguish muons and electrons, which had been well established for the earlier atmospheric neutrino results. As such, the primary background for K2K was events containing a π^0 from a NC interaction. This background occurs when one of the two gammas from the π^0 decay is not reconstructed, due to highly asymmetric energies or a small opening angle between the two gammas. Beam ν_e events are around 1% at the KEK site and the background from such electron neutrinos intrinsic to the beam was estimated to be only 13% of the total background.

At the limit set by the CHOOZ experiment [12] and with an exposure of 9.2×10^{19} protons on target, K2K expected to see only a few events and so it was critical that the background was reduced to a very low level. The basic selection of electron neutrino events is as follows: the first step is to require electron Čerenkov-ring candidates; secondly, any events with electron-equivalent energy below 100 MeV are removed to reject charged pions and electrons from muon decay; and thirdly, no candidate may have a muon decay within a 30 μ s time window. To improve the rejection of the π^0 background a dedicated algorithm to calculate the invariant mass under the assumption that there were two rings was also used. The total background expectation with the above cuts was $1.7_{-0.4}^{+0.6}$ events (in the case of no oscillation). The overall efficiency for selection of ν_e signal events in the simulation is around 50%.

The fraction of the background coming from NC interactions that produce a single π^0 (NC $1\pi^0$) was 70% so constraining the associated systematic uncertainty was crucial. To do this a 1 kiloton water Čerenkov Near detector was used to measure the NC $1\pi^0$ /CC interaction ratio and the uncertainty was constrained to the 12% level. Many other sources of systematic uncertainty were considered and the largest individual one concerned the π^0 mass cut and that uncertainty was constrained using atmospheric neutrino data. The other systematics also included the detector efficiency, water properties, neutrino flux at SK, and several neutrino interaction model uncertainties. In total the background uncertainty was between 24–39% depending on the run period.

K2K observed 1 event that passed their selection criteria, consistent with the background expectation. These data allowed a 90% C.L. limit to be set on the maximum electron neutrino appearance probability of 0.13, at the oscillation parameters measured by K2K via ν_μ disappearance (see section 4.1). Such an appearance probability corresponds to an approximate limit of $\sin^2(2\theta_{13}) < 0.26$.

5.2. MINOS ν_e Appearance Results

The first MINOS ν_e appearance result was released in 2009 [57] and two further results with more data and analysis improvements have since been published [58, 59]. The MINOS detectors were optimized for measuring muon neutrino interactions at the few-GeV scale. The steel planes are 1.4 radiation lengths thick and the strip width is 4.1 cm (compared to the Molière radius of 3.7 cm) giving a relatively coarse view of an electron shower. Absolutely crucial for controlling the systematic uncertainties on these measurements is the functionally identical design of the Near and Far detectors. As with K2K, the dominant background is from NC interactions. Although, ν_μ CC events also contribute significantly to the background along with intrinsic ν_e events in the beam and ν_τ events that have oscillated from ν_μ .

Determining the composition of the background is important for this analysis since at the Far detector a fraction of the ν_μ events have oscillated away and therefore the background from ν_μ CC events is reduced. The other effect of oscillations is to introduce a background from ν_τ in the Far detector that does not exist in the Near detector. In contrast, the NC events do not oscillate away and to first order that background component is the same in the Near and Far detectors. MINOS took a data-driven approach to determining the background composition

by comparing the data with the simulation for a number of data sets taken with the NuMI beam in special configurations. For example, with the magnetic horns turned off the peak in the energy spectrum disappears, which drastically changes the CC/NC ratio as a function of energy. Similarly, data taken with the beam configured to produce higher energy neutrinos has an enhanced NC fraction at low energies. A fit to the ND data and MC across all these special data sets was used to estimate the background composition and determine the uncertainties on each component.

The selection of electron neutrino candidate events starts out with fiducial volume cuts and ensuring the event is in time with the low-duty-cycle NuMI beam. Electron showers penetrate only a few (typically 6–12) planes and are transversely compact so any events with tracks longer than 24 planes or with a track extending more than 15 planes beyond the end of a reconstructed shower are rejected. A requirement is also made that events contain at least 5 contiguous planes with an energy deposition at least half that of a minimum ionizing particle. Any events with an energy less than 1 GeV or greater than 8 GeV are also removed. After these pre-selection cuts 77% of the signal, 39% of NC events and 8.5% of ν_μ CC events remain.

Further reduction of backgrounds is achieved by a more sophisticated analysis of the energy deposition patterns in preselected events. The first two MINOS results used an artificial neural network with 11 variables characterizing the transverse and longitudinal profile of events. For the most recent MINOS analyses, a nearest-neighbor “library event matching” (LEM) technique is used. Each data event is compared, one-by-one, to a large library of tens of millions of simulated events. Since the detector is homogeneous, events occurring throughout the volume are translated to a fixed reference location and then compared at the level of individual strips. This approach is computationally intensive and is made more manageable in two notable ways: firstly, fluctuations in the energy deposition of individual strips are allowed for; and secondly, library events are shifted by ± 1 plane in search of a better match. The final LEM discriminant is formed using a neural network that takes as its inputs the event energy along with three variables derived from the 50 best-matched events. A cut of $\text{LEM} > 0.7$ selects $(40.4 \pm 2.8)\%$ of signal events.

The predictions for the Far detector signal and backgrounds as a function of energy and LEM uses the Near detector data as the starting point. The simulated ratio of Near and Far detector rates for each background type is used as the conversion factor to translate the Near detector data into a Far detector prediction.

Two data samples provide sidebands that allow many of the procedures developed for this analysis to be tested and the accuracy of the simulation to be probed. Firstly, ν_μ CC events with cleanly identified muons provide a sample of known hadronic showers once the muon hits are removed. These muon-removed events are a lot like NC interactions and the predicted and observed events at the Far detector agree well. The second sideband is the $\text{LEM} < 0.5$ region that contains almost no ν_e appearance events. The Far detector prediction for this $\text{LEM} < 0.5$ region is obtained in the same way as for the signal region and so all stages of the analysis up to the final signal extraction are exercised: for example, determining the background composition and extrapolating the Near detector data is done in the same way.

A fit to the data, binned as a function of the LEM discriminant and reconstructed energy, was performed using the full 3-flavor oscillation framework including matter effects. The influence of the already measured oscillation parameters was included when constructing the contours.

Updated MINOS results were released this summer for neutrinos, along with the first appearance results for antineutrinos [45]. With an exposure of 10.6×10^{20} POT in the neutrino-enhanced beam and assuming $\sin^2 2\theta_{13} = 0$ ($\sin^2 2\theta_{13} = 0.1$, $\delta = 0$, normal mass hierarchy) MINOS expected to see 128.6 (161.1) events in the Far detector; 152 events were observed.

With an exposure of 3.3×10^{20} POT in the antineutrino-enhanced beam and assuming $\sin^2 2\theta_{13} = 0$ ($\sin^2 2\theta_{13} = 0.1$, $\delta = 0$, normal mass hierarchy) MINOS expected to see 17.5

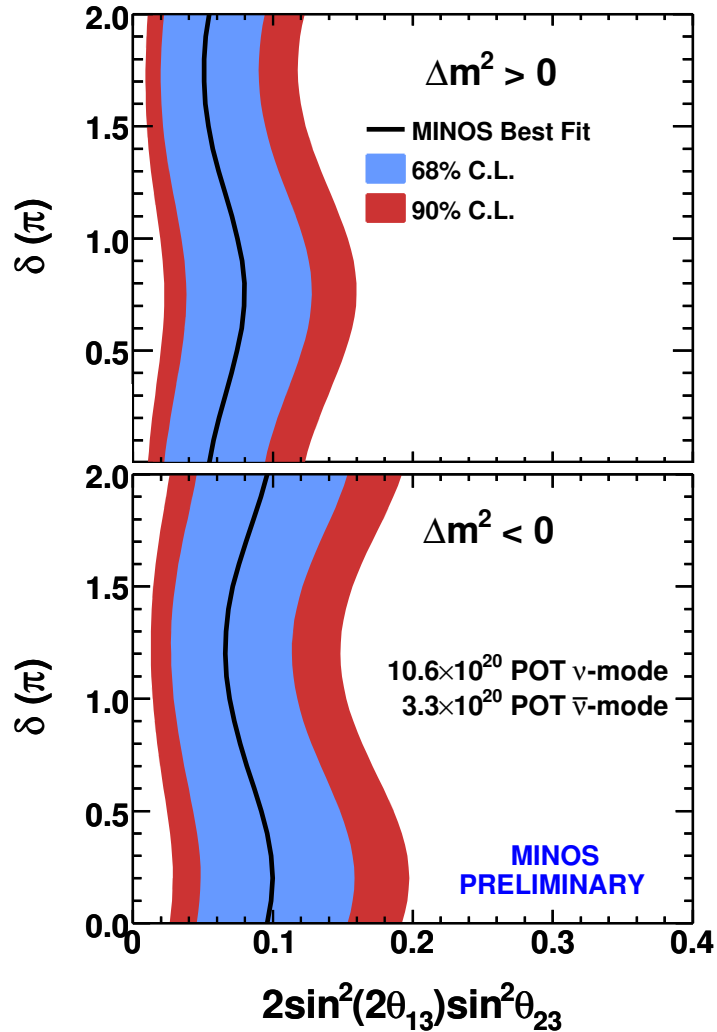


Figure 18. MINOS allowed regions for the CP violating phase and $2 \sin^2(2\theta_{13}) \sin^2 \theta_{23}$, obtained using the full data set of both neutrinos and antineutrinos. The top (bottom) plot assumes the normal (inverted) mass hierarchy. All values of the CP violating phase are consistent with the data and so the best fit parameters are shown by the black line. The blue (red) band shows the regions allowed at 68% (90%) confidence level. The $\theta_{13} = 0$ hypothesis is disfavored at the 96% confidence level. These results were preliminary at the time of writing [45].

(21.2) events in the Far detector; 20 events were observed.

The allowed regions as a function of the CP violating phase, δ , and $2 \sin^2(2\theta_{13}) \sin^2 \theta_{23}$ are shown in Figure 18. For $\delta = 0$ and the normal (inverted) mass hierarchy a best fit of $2 \sin^2(2\theta_{13}) \sin^2 \theta_{23} = 0.053$ (0.094) is obtained; the 90% C.L. allowed range is $0.01 < 2 \sin^2(2\theta_{13}) \sin^2 \theta_{23} < 0.12$ ($0.03 < 2 \sin^2(2\theta_{13}) \sin^2 \theta_{23} < 0.19$) and the $\theta_{13} = 0$ hypothesis is disfavored at the 96% confidence level. These results are consistent with both the T2K result described below in section 5.3 and with the reactor neutrino experiments.

Figure 19 shows the results from the first measurement of electron antineutrino appearance. The data set used for this measurement was obtained with the NuMI beam set to enhance production of antineutrinos. The limits on $2 \sin^2(2\theta_{13}) \sin^2 \theta_{23}$ are consistent with those from

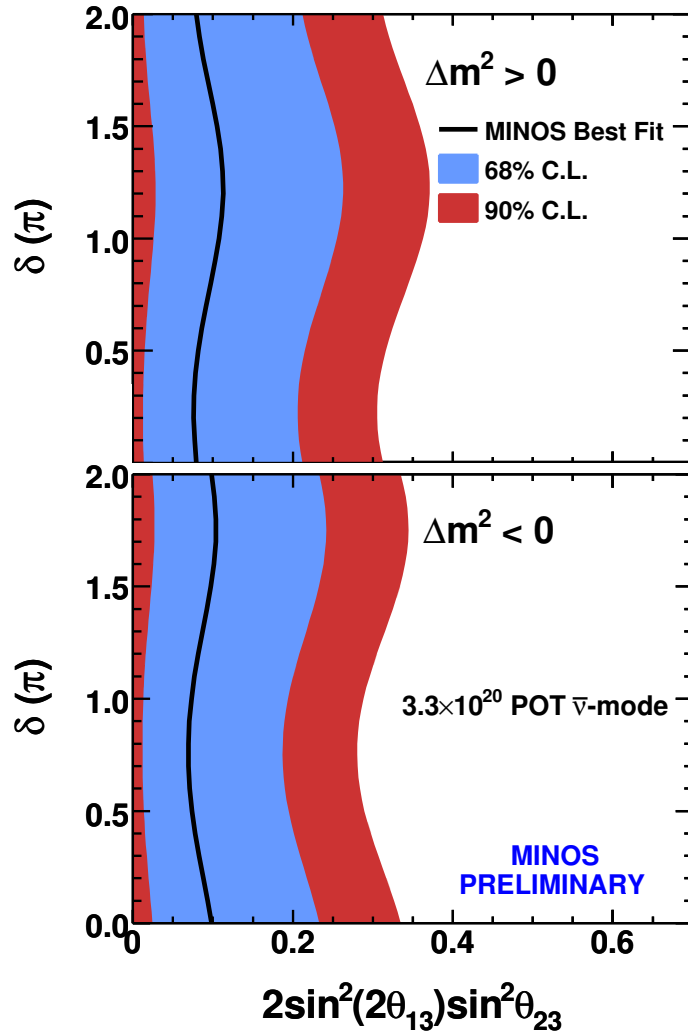


Figure 19. MINOS allowed regions for antineutrinos as a function of the CP violating phase and $2\sin^2(2\theta_{13})\sin^2\theta_{23}$. See Figure 18 for the full description. These results were preliminary at the time of writing [45].

neutrinos. Although, the smaller exposure and lower antineutrino cross-section means that the limits are not as strong as for neutrinos. Significant improvement in measurement of electron antineutrino appearance is not expected until NO ν A takes data using the NuMI beam configured for enhanced $\bar{\nu}_\mu$ production (see section 7).

5.3. T2K ν_e Appearance Results

The primary goal of the T2K experiment is to discover electron neutrino appearance and precisely measure the oscillation probability if it exists. The experimental setup is optimized for this purpose.

T2K reported the first evidence of electron neutrino appearance (2.5σ significance, p-value = 0.7%) in June 2011 based on 1.43×10^{20} POT data taken before the Great East Japan Earthquake on 11th March 2011 [60].

The goal of the analysis is to select ν_e CC interactions at high efficiency and with the

background contamination as low as possible. At the peak of the T2K neutrino energy spectrum, around 600 MeV, the interaction of neutrinos is dominated by CC quasi-elastic interaction (CCQE), $\nu_e + n \rightarrow e^- + p$, and that was chosen as the target signal interaction. The benefit of CCQE interaction is that with just a measurement of the momentum of the final lepton, the parent neutrino energy can be reconstructed with a good energy resolution of around 80 MeV.

The signature for signal events in the Super-Kamiokande detector is a single showering (electron-like) ring in the expected energy region. The two major sources of background events are the intrinsic electron neutrino contamination in the beam mainly produced by muon decay in the decay volume, and inelastic NC interaction of all flavors that contain a π^0 in the final state. The γ s from π^0 s are detected in SK by the Čerenkov light from their electromagnetic showers, which can be indistinguishable from the Čerenkov light distribution produced by an electron. For example, if one of the two γ s from the π^0 decay is missed, the event topology in SK becomes very similar to that of the signal, i.e. a single electron-like ring.

Selection criteria for the signal event are as follows. The “fully contained in fiducial volume” (FCFV) events are selected by requiring: no event activity in either the outer detector or in the 100 μ s before the event trigger time; at least 30 MeV electron-equivalent energy deposited in the inner detector (defined as visible energy E_{vis}); and the reconstructed vertex to be in the fiducial volume of 22.5 kilotonnes. The event timing is required to be within the range from -2 μ s to 10 μ s around the beam trigger time.

Further selection cuts require events with the number of rings equal to 1 and a PID consistent with being electron-like. The visible energy is required to be $E_{vis} > 100$ MeV to reduce NC elastic-interactions and decay electron backgrounds. It is also required to have no associated delayed electron signal to reduce the background from invisible $\pi \rightarrow \mu$ decay. To suppress misidentified π^0 , a second electron-like ring is forced to be reconstructed and a cut on the two-ring invariant mass $M_{inv} < 105$ MeV/ c^2 is imposed. Finally, the neutrino energy E_ν^{rec} , computed using the reconstructed momentum and direction of the ring assuming CCQE kinematics and neglecting Fermi motion, is required to be $E_\nu^{rec} < 1250$ MeV.

The ν_e appearance signal efficiency is estimated with MC to be 66% while rejection for $\nu_\mu + \bar{\nu}_\mu$ CC, beam ν_e CC, and NC are $> 99\%$, 77% , and 99% , respectively.

The selection is applied to the data and 6 events in SK are selected as signal candidates from all data before the earthquake, corresponding to 1.43×10^{20} POT. The E_ν^{rec} distribution of the observed events together with the signal and background expectations are shown in Figure 20.

The expected signal and background events are estimated using the far detector MC simulation with the constraints and inputs from measurements of near detector ν_μ CC events and external data. These external data include hadron production measurements made by the NA61 experiment [61, 62] using 30 GeV protons impinging on the neutrino production target and also neutrino interaction cross-sections measured by previous experiments such as MiniBooNE.

The off-axis near detector measures the number of inclusive ν_μ CC events by selecting events with a single negative muon. The ratio of the observed number of events to that from the MC simulation is $1.036 \pm 0.028(\text{stat})_{-0.037}^{+0.044}(\text{det.syst}) \pm 0.038(\text{phys.syst})$. This near detector ratio is multiplied by the number of events from the far detector simulation to give the predicted number of events in the far detector data. This method provides partial cancellation of uncertainties in the absolute flux and cross-sections at the far detector.

The number of background events thus obtained when $\sin^2(2\theta_{13}) = 0$ is estimated to be 1.5 ± 0.3 (syst). The major contributions to the background systematic error come from the beam flux (8.5%), cross-section (14%) and far detector systematic error (15%). The probability that the observed number of events becomes 6 or larger if $\sin^2(2\theta_{13}) = 0$ is calculated to be 0.7%, which corresponds to a 2.5σ excess.

The constraints on the oscillation parameters are evaluated also by using only the number of events. The confidence intervals are $0.03(0.04) < \sin^2 2\theta_{13} < 0.28(0.34)$ at 90% C.L. and

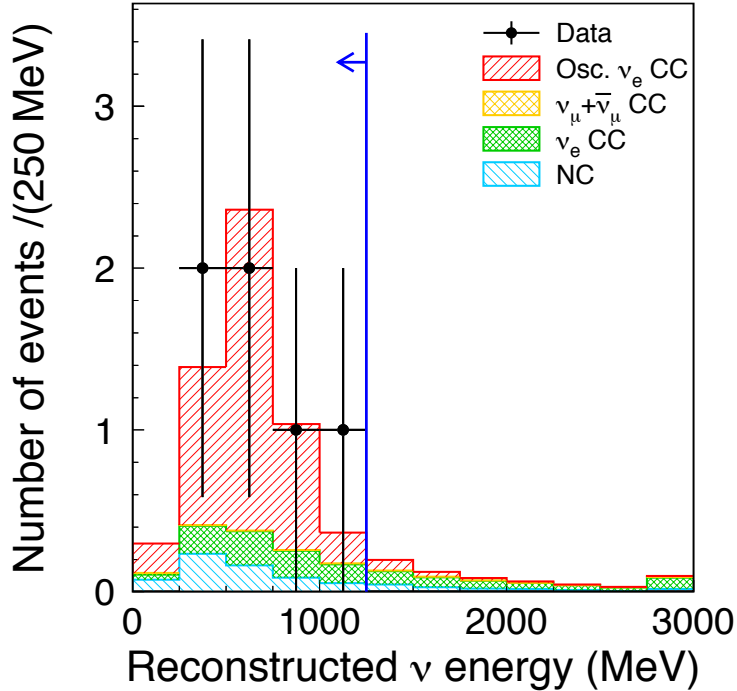


Figure 20. Reconstructed neutrino energy E_ν^{rec} spectra for T2K ν_e appearance search. The black points show the 6 candidate events observed in SK using 1.43×10^{20} POT data. Using $\sin^2(2\theta_{13}) = 0.1$ the red histogram is the predicted appearance signal, the expected background shown in yellow is for muon neutrinos, green is for the electron neutrinos intrinsic to the beam and blue is for the NC events.

the best fit parameters are $\sin^2(2\theta_{13}) = 0.11(0.14)$ for the normal (inverted) hierarchy assuming $\sin^2(2\theta_{23}) = 1$, $\Delta m_{32}^2 = 2.4 \times 10^{-3} \text{ eV}^2$ and $\delta = 0$. Figure 21 shows the T2K allowed regions of parameters in the $\sin^2 2\theta_{13}$ - δ plane.

To summarize the T2K ν_e appearance search, 6 signal candidate events are detected while the expected number of background events at $\sin^2(2\theta_{13}) = 0$ is 1.5 ± 0.3 . The probability to observe 6 or more events without ν_e appearance is 0.7%, which corresponds to 2.5σ significance¹. Constraints on the $\sin^2 2\theta_{13}$ - δ space are given for both the normal and inverted mass hierarchy.

6. Results on New Physics Searches

The provision of intense and relatively well understood neutrino beams along with large detectors has opened up whole new avenues to look for new physics. Here we focus on three main areas: section 6.1 describes the searches for sterile neutrinos; section 6.2 briefly summarizes neutrino velocity measurements; and section 6.3 describes searches for Lorentz symmetry violation.

6.1. Searches for sterile neutrinos

While the conventional picture of oscillations between three active neutrino flavors is well established, the possibility of mixing with one or more unseen sterile neutrinos is not excluded. Neutral-current (NC) interaction cross-sections are identical for the three active flavors and so no change in the NC event rate would be observed as a function of L/E in the standard neutrino

¹ In Summer 2012, T2K updated the results with 3.01×10^{20} POT of data [63]. The observed number of events is 11 while the expected background is 3.22 ± 0.43 at $\sin^2(2\theta_{13}) = 0$, which corresponds to 3.2σ significance and provides further firm evidence of ν_e appearance.

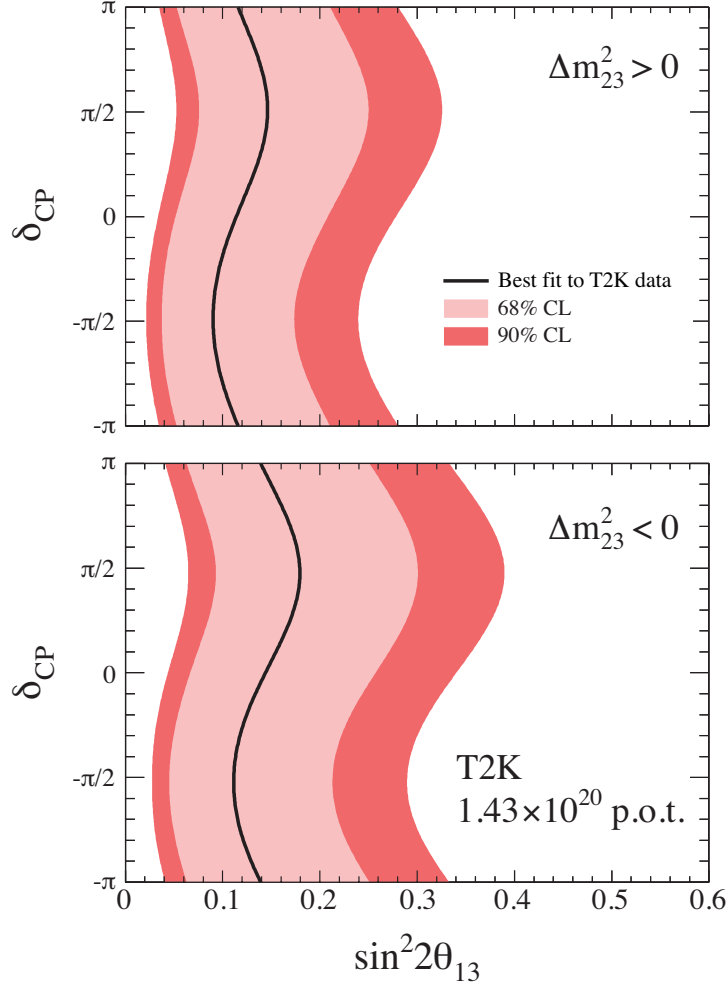


Figure 21. Allowed regions in the $\sin^2 2\theta_{13}$ – δ plane from the T2K ν_e appearance measurement. Light (dark) red areas are 68% C.L. and 90% C.L. regions. Solid black curves are best fit relations.

model. MINOS provided the first limits on the fraction of mixing to sterile neutrinos allowed at the atmospheric mass splitting in [64], with details given in a longer paper [65]. Earlier, in 2000, Super-Kamiokande had excluded the possibility of maximal $\nu_\mu \rightarrow \nu_s$ oscillations at 99% C.L. [66] by exploiting the effect such oscillations would have on both the NC event rate and the number of ν_μ and ν_τ candidate events (the difference in the neutrino-matter interaction of ν_μ and ν_τ compared to ν_s is significant for atmospheric neutrinos of the energy measured by SK). More recent observations of ν_τ appearance [53, 54] also constrain oscillations to sterile neutrinos, although limits are not directly given in those papers. The current best limits on the fraction of mixing to sterile neutrinos are from MINOS and given in [67].

Selection of NC events in the MINOS detectors requires careful study since the visible energy is relatively low and there is no distinct feature to the events (for example, missing transverse momentum is not easily observed in the MINOS detectors). NC candidate events can have signal in as few as 4 scintillator strips. The high rate environment of the ND, where there are around 16 events per 10 μ s beam spill, requires additional selections on timing and topology: events must be separated by at least 40 ns and events that occur within 120 ns of each other must be separated in the beam direction by at least 1 m. To select an NC-candidate event sample the

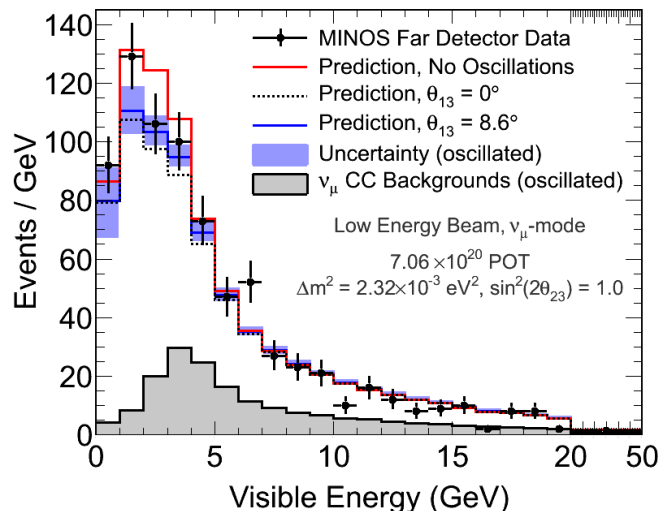


Figure 22. Visible energy spectrum of MINOS Far detector neutral-current event candidates [45]. The data are shown by the black points. The prediction obtained from the Near detector data is shown for three cases: no oscillations (red); oscillations with atmospheric parameters and $\theta_{13} = 8.6^\circ$ (dashed black); and oscillations with atmospheric parameters and $\theta_{13} = 0^\circ$ (dotted black). The contamination of the NC spectrum from ν_μ CC events is shown by the gray histogram.

length of the event has to be less than 60 planes and any track in the event must not extend beyond the end of a shower by more than 5 consecutive planes.

An extrapolation procedure similar to that used in the ν_e appearance analysis (see section 5.2) is used to form the Far detector prediction for the NC spectrum. Figure 22 shows the visible energy spectrum of Far detector candidate NC events. The data can be seen to be consistent with no oscillation to sterile neutrinos.

Many sources of systematic uncertainty on the MINOS NC results are similar to the ν_μ disappearance and ν_e appearance measurements (see sections 4.1.2 and 5.2 respectively), for example the absolute and relative energy scale of hadronic showers, and the relative event rate normalization. Uncertainties specific to the NC measurement are in the Near and Far detector selection, and in the CC background. The latest results, given below, are approaching the systematic limit for how much further these measurements can be improved by MINOS.

A straightforward phenomenological approach to presenting the limits on the allowed level of sterile neutrino mixing is to consider the fraction, f_s , of the disappearing ν_μ flux that could oscillate to ν_s . MINOS finds $f_s < 0.22$ (0.40) at 90% C.L., where the number in brackets is the limit assuming maximal ν_e appearance at the CHOOZ limit. The alternative approach to presenting the limits is in the context of a specific model. MINOS has considered two models: firstly, one where the fourth mass eigenstate $m_4 = m_1$; and secondly where $m_4 \gg m_3$. The 90% C.L. limits obtained from MINOS data are $\theta_{24} < 7^\circ$ (8°) and $\theta_{34} < 26^\circ$ (37°) in the $m_4 \gg m_3$ model, and $\theta_{34} < 26^\circ$ (37°) in the $m_4 = m_1$ model. In the future, the MINOS+ experiment will extend the sensitivity to sterile neutrinos, in particular through also constraining the disappearance of ν_μ and $\bar{\nu}_\mu$ (see section 7.2).

6.2. Neutrino Velocity

In 2007 MINOS made the first measurement of neutrino velocity in a long-baseline experiment [68]. The time of flight between the Near and Far detectors separated by 734298.6 ± 0.7 m was measured to be $-126 \pm 32(\text{stat}) \pm 64(\text{syst})$ ns w.r.t. the calculated time for light to travel the same distance, which corresponds to $(v - c)/c = (5.1 \pm 2.9) \times 10^{-5}$. This result was systematically limited by uncertainties in the timing system and its overall sensitivity comparable with previous neutrino velocity measurements from short-baseline experiments [69].

Dedicated upgrades to the OPERA experiment's timing system along with high statistics neutrino event samples gave substantially improved sensitivity to the neutrino velocity. In September 2011 they released their result $(v - c)/c = [2.37 \pm 0.32(\text{stat})_{-0.24}^{+0.34}(\text{syst})] \times 10^{-5}$ [70], which generated huge world wide media interest. However, in February 2012 the OPERA collaboration released a statement, available on their website, saying that two errors in the timing system had been found that could potentially bring the neutrino velocity back into line with expectations from special relativity. This was followed by a measurement from the ICARUS experiment [71], also located in the LNGS laboratory, that was of similar sensitivity to OPERA but consistent with expectations. Around the time of writing OPERA released an updated result $(v - c)/c = [0.27 \pm 0.31(\text{stat})_{-0.33}^{+0.34}(\text{syst})] \times 10^{-5}$ [70], confirming that they had understood the anomaly in their first result. Results from Borexino [72] and LVD [73] are also consistent with OPERA and ICARUS. These results from four of the experiments located at Gran Sasso are the world's most precise measurements of the neutrino velocity and they are approaching their ultimate systematic limit. Future measurements that use different beamlines and hence have a lower number of correlated systematic uncertainties will be important. MINOS, and in future MINOS+, will exploit recent investments in their timing systems with the aim of reducing the systematic uncertainties further [74].

6.3. Searches for Lorentz Symmetry Violation

MINOS has investigated whether neutrinos have a preferred direction in space and hence violate Lorentz symmetry and consequently also CPT symmetry. This search was performed in the context of the Standard Model Extension theory [75, 76, 77] that provides a model-independent framework with coefficients to quantify the various ways Lorentz symmetry could be violated. The experimental observable for these searches is a sidereal variation in the rate of neutrino interactions. MINOS has results for ν_μ and $\bar{\nu}_\mu$ in the Near detector as well as ν_μ in the Far detector [78, 79, 80].

The rotation of the Earth rotates the neutrino beam in the sun-centered inertial reference frame with the sidereal frequency of $2\pi/23^{\text{h}}56^{\text{m}}04.09053^{\text{s}}$. The offset of the sidereal frequency from the Earth's rotational frequency of $2\pi/24^{\text{h}}$ is experimentally advantageous since diurnal effects can potentially average out over the course of a year. The MINOS analysis was performed by examining the data as a function of local sidereal phase (LSP), which is simply the local sidereal time divided by the length of a sidereal day. Each neutrino event was placed in an LSP histogram and the protons on target for each beam spill used in the analysis were placed in a second LSP histogram. The ratio of the two histograms gave the normalized number of neutrino events observed as a function of LSP. Fast Fourier transforms to determine the power associated with sinusoidal functions at the sidereal frequency and its second harmonic were performed. To date, no sidereal variation of the neutrino event rate has been detected.

In addition to long-baseline accelerator experiments, searches for Lorentz symmetry violation have been performed by several other neutrino experiments. This has allowed many of the coefficients in the SME to be constrained over a wide range of directions, baselines and neutrino energies. A comprehensive summary of experimental limits is given in [81].

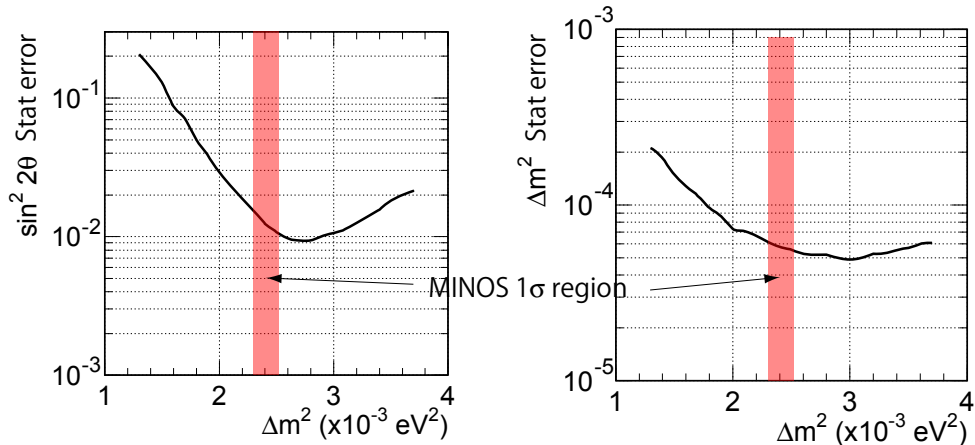


Figure 23. T2K expected statistical precision on the oscillation parameters $\sin^2(2\theta_{23})$ and $|\Delta m_{32}^2|$ assuming an exposure of $750 \text{ kW} \times 5 \times 10^7$ seconds as a function of true $|\Delta m_{32}^2|$ [82]. The 1σ confidence intervals for $|\Delta m_{32}^2|$ from MINOS are indicated by red hatches.

7. Future Sensitivities

The expected future physics sensitivities of experiments currently running, or about to start taking data, are outlined here. Section 7.1 describes the prospects for measurements of the standard 3-flavor neutrino oscillation parameters and section 7.2 focuses on models of new physics.

7.1. Oscillation physics

As of 2012, all three mixing angles are known to be nonzero and have been measured to reasonably good accuracy. However, there is no significant information on the mass ordering, the θ_{23} octant or CP violation yet. The main goals of long-baseline experiments in the next decade will be to determine or obtain indications of the present unknowns by improving the precision of the measurements as much as possible. Since the CP violation term in the ν_e appearance probability depends on all the mixing angles in some way, it is important to improve the precision of θ_{23} through ν_μ disappearance measurements as well as ν_e appearance. Further, if $\sin^2(2\theta_{23})$ is not unity, then the determination of the θ_{23} octant will tell us whether ν_3 couples more strongly to ν_μ or ν_τ .

T2K plans to accumulate up to $750 \text{ kW} \times 5 \times 10^7$ seconds equivalent POT, which is about 8×10^{21} POT and 26 times the exposure so far. The NO ν A sensitivities discussed below all assume that NO ν A will run for three years in neutrino mode and three years in antineutrino mode, for a total of 36×10^{20} POT. These predicted sensitivities are largely based on analysis techniques that were used by the MINOS experiment. NO ν A expects to be able to achieve somewhat better sensitivities as it incorporates additional techniques allowed by NO ν A's finer segmentation and greater active fraction.

7.1.1. ν_μ Disappearance

The disappearance of ν_μ charged current events measures $\sin^2(2\theta_{23})$ and $|\Delta m_{32}^2|$. The expected statistical precision of the T2K ν_μ disappearance measurements at $750 \text{ kW} \times 5 \times 10^7$ seconds are plotted in Figure 23 [82]. The statistical precision reaches $\delta(\sin^2 2\theta_{23}) \sim 1\%$ and $\delta(|\Delta m_{32}^2|) \sim 0.05 \times 10^{-3} \text{ eV}^2$. The goal for the systematic uncertainties is to reach the same level as for the statistical errors for both of the parameters.

The latest MINOS measurement of $\sin^2(2\theta_{23})$ is 0.96 ± 0.04 [45]. For the reasons cited above,

NO ν A should be able to make a measurement that is about a factor of two to three more sensitive. Figure 24 shows the NO ν A sensitivity for three possible values of $\sin^2(2\theta_{23})$. NO ν A will gain further information about θ_{23} from $\nu_\mu \rightarrow \nu_e$ oscillations, as discussed below.

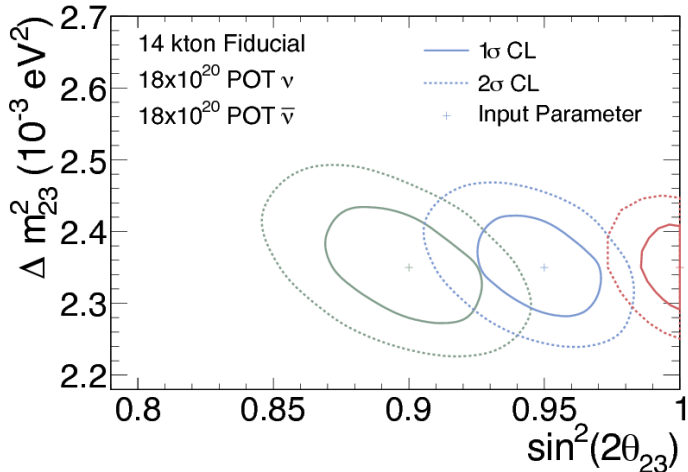


Figure 24. One and two standard deviation NO ν A sensitivity contours for a joint measurement of $|\Delta m_{32}^2|$ and $\sin^2(2\theta_{23})$ for three possible values of these parameters indicated by the plus signs. The single parameter measurement of $\sin^2(2\theta_{23})$ will be somewhat more sensitive than the extreme limits of the displayed contours.

7.1.2. $\nu_\mu \rightarrow \nu_e$ Oscillations

The parameters for $\nu_\mu \rightarrow \nu_e$ oscillations are considerably more complex than for ν_μ disappearance. This process is largely proportional to both $\sin^2(2\theta_{13})$ and $\sin^2(2\theta_{23})$, with large perturbations caused by the mass ordering (through the matter effect) and by CP violation. A convenient way to see the dependences is through bi-probability plots. These plots show the loci of possible NO ν A measurements of $\nu_\mu \rightarrow \nu_e$ and $\bar{\nu}_\mu \rightarrow \bar{\nu}_e$ oscillation probabilities, given a set of parameters. These parameters include $\sin^2(2\theta_{13})$, which is fixed at 0.095, a value consistent with the recent reactor measurements[83, 84, 18], and $\sin^2(2\theta_{23})$. Figures 25 and 26 show bi-probability plots for $\sin^2(2\theta_{23}) = 1.00$ and 0.97, respectively. The CP-violating phase δ traces out the ovals and the multiplicity of ovals represents the two possible mass orderings and, for Figure 26, the ambiguity of whether θ_{23} is larger or smaller than $\pi/4$.

A useful way to visualize what NO ν A will be able to do is to superimpose one and two standard deviation contours on the bi-probability plots. For example, Figures 27 and 28 show these contours for a favorable set of parameters, normal mass ordering and $\delta = 3\pi/2$. The mass ordering is resolved to more than two standard deviations, the θ_{23} ambiguity is resolved to two standard deviations, and CP violation is established to almost two standard deviations. This occurred because the matter effect and the CP-violating effect went in the same direction, so there was no ambiguity.

An unfavorable set of parameters would be one in which the matter effect and the CP-violating effect go in opposite directions so that there is an ambiguity as to which direction each one went. An example of that is shown in Figure 29. The θ_{23} ambiguity is resolved, but the mass ordering is not, and therefore there is little information on the CP-violating phase. If nature gives us this situation, then the only way to resolve the mass ordering in the short term is to compare NO ν A measurements of $\nu_\mu \rightarrow \nu_e$ oscillations with those from an experiment with a different baseline. The only experiment that meets that requirement is T2K, which has a 295 km baseline.

The algorithm for resolving the mass ordering is quite simple. If NO ν A measures a higher probability of $\nu_\mu \rightarrow \nu_e$ oscillations than T2K, then the mass ordering is normal; if it is the opposite, it is inverted. That is because NO ν A and T2K will see the identical CP-violation,

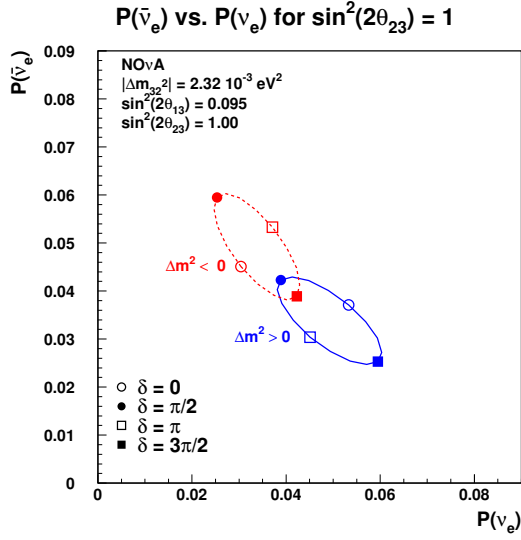


Figure 25. Bi-probability plot for $\sin^2(2\theta_{23}) = 1.00$. See text for explanation.

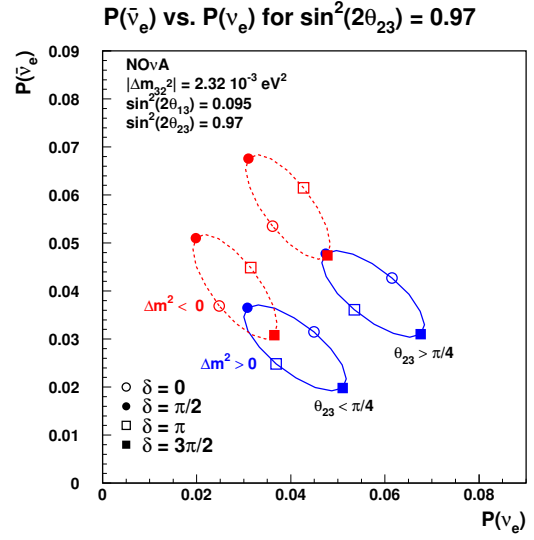


Figure 26. Bi-probability plot for $\sin^2(2\theta_{23}) = 0.97$. See text for explanation.

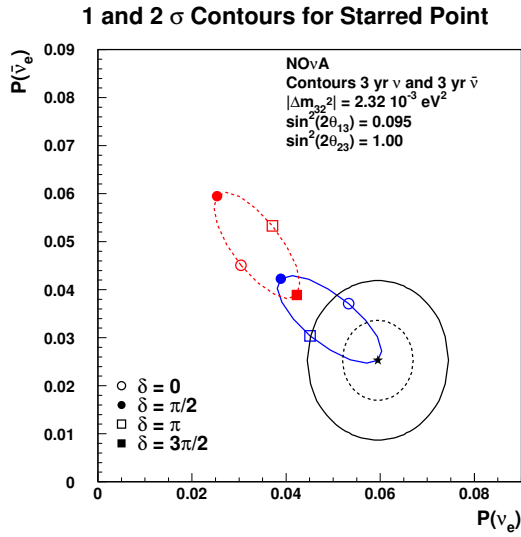


Figure 27. Bi-probability plot for $\sin^2(2\theta_{23}) = 1.00$ with NO ν A expected 1 and 2 standard deviation contours superimposed on the starred point.

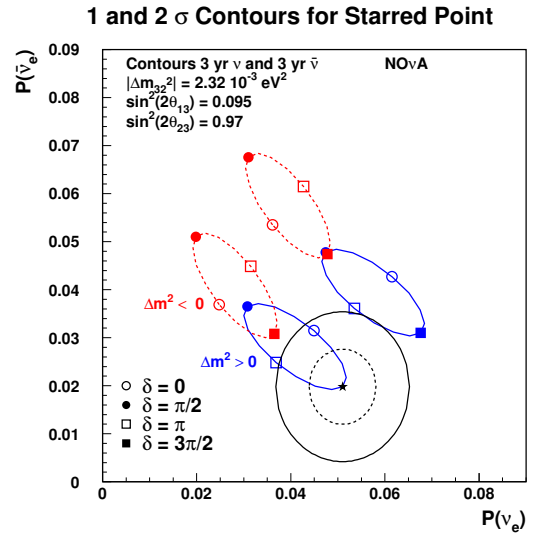


Figure 28. Bi-probability plot for $\sin^2(2\theta_{23}) = 0.97$ with NO ν A expected 1 and 2 standard deviation contours superimposed on the starred point.

but T2K will see a much smaller matter effect due to its shorter baseline. The only catch in this algorithm is that the comparison must be done at the same point in the oscillation phase, and the two experiments run at different average oscillation phases. Figures 30 and 31 show the bi-probability plots in which the NO ν A measurements have been extrapolated to the same oscillation phase as the T2K measurements. A comparison of the two plots shows that the

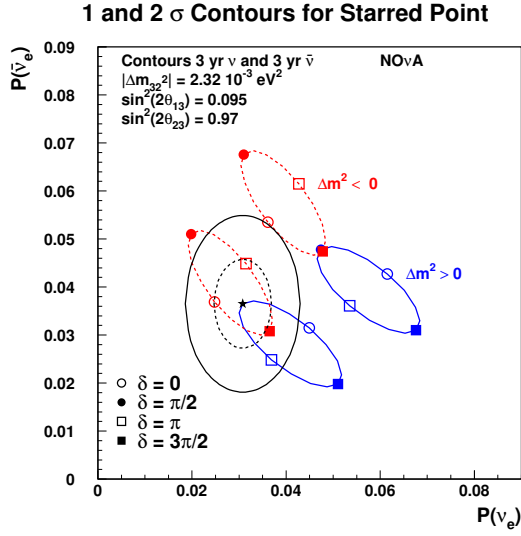


Figure 29. Bi-probability plot for $\sin^2(2\theta_{23}) = 0.97$ with NO ν A expected 1 and 2 standard deviation contours superimposed on the starred point.

algorithm works for all values of δ .

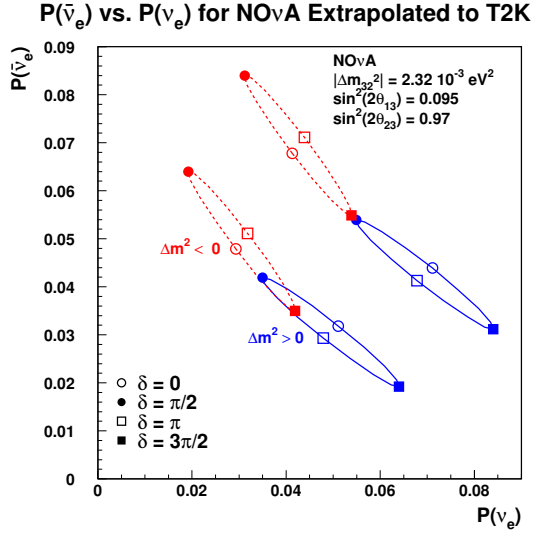


Figure 30. Bi-probability plot for $\sin^2(2\theta_{23}) = 0.97$ with NO ν A extrapolated to the average oscillation phase of T2K

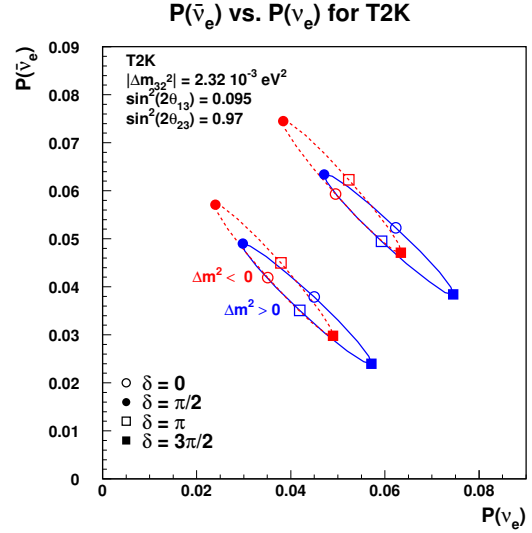


Figure 31. Bi-probability plot for $\sin^2(2\theta_{23}) = 0.97$ for T2K.

Unfortunately, the combined statistical power of NO ν A and T2K at the end of the nominal six-year NO ν A run will be insufficient to resolve the mass ordering at the two standard deviation level using this strategy. However, it is unlikely that either the American or the Japanese neutrino program will end at that time. With anticipated improvements in both programs, in the worst case, the mass ordering should be resolved in the next decade. Figures 32 and 34 summarize the NO ν A sensitivities for resolving the mass ordering and determining that there is CP violation in the leptonic sector, respectively. These figures are for NO ν A alone and use only

the total measured oscillation rate. There will be some gain in sensitivity in using the measured energy dependence and, as mentioned previously, improvements in the analysis. Figures 33 and 35 show the same information, but include the information from T2K that is expected to be available at the end of the nominal six-year $\text{NO}\nu\text{A}$ run.

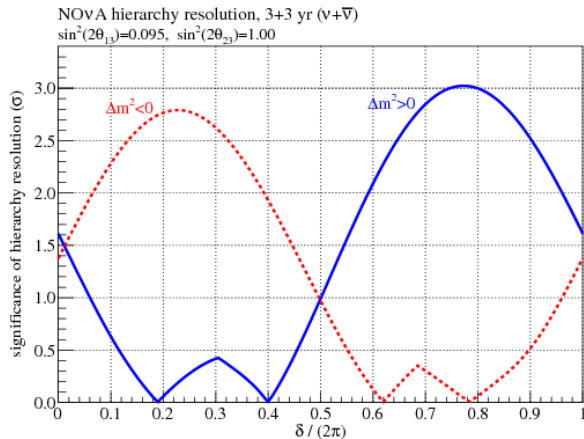


Figure 32. Significance of the resolution of the mass ordering as a function of δ in standard deviations. These sensitivities are for $\text{NO}\nu\text{A}$ alone for the two possible orderings and $\sin^2(2\theta_{23}) = 1.0$. The zeros correspond to the crossing of the ovals in Figure 25.

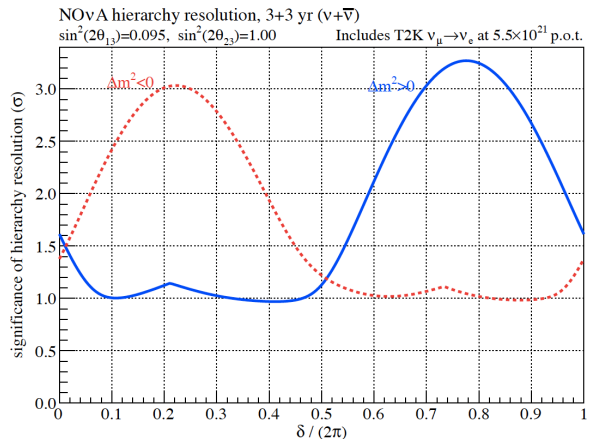


Figure 33. Same as the figure to the left except that information from the T2K experiment has been included.

7.2. Searches for new physics

Future data to be accumulated by long-baseline experiments offer novel avenues to search for new physics in several ways. MINOS+ [19] will run with the NuMI beam providing a flux that is least a factor of two higher in energy and power than for MINOS. This wide band beam will yield thousands of interactions a year in the Far detector with well measured L/E . In combination with a precise prediction for the spectrum of interactions from the Near detector, precision probes of new physics will be performed. $\text{NO}\nu\text{A}$ and T2K experiments will exploit their narrow band beams that have well defined energies. The $\text{NO}\nu\text{A}$ detectors with their fine granular sampling of events (1 plane is 0.15 radiation lengths, see section 3.7) will provide enhanced ability to distinguish the different neutrino interaction types.

Sterile neutrinos are one of the major areas of interest that will be probed by upcoming experiments. $\text{NO}\nu\text{A}$ will improve on the MINOS searches for a deficit in the rate of NC interactions in the Far detector (see section 6), with significantly better rejection of the dominant background coming from ν_μ CC events. In addition to studies of NC events, MINOS+ will use the complementary approach to looking for sterile neutrinos that involves constraining the disappearance of ν_μ and hence, via unitarity, will constrain the appearance of ν_e (that short-baseline experiments are directly sensitive to). Figure 36 shows what MINOS+ expects to add to the world's constraints on muon-electron mixing at mass squared splittings between 10^{-2} eV^2 and 10 eV^2 (i.e. larger than the atmospheric and solar mass splittings). The red curve in Figure 36 is the expected combined sensitivity of MINOS+ and the Bugey reactor experiment [85]: Bugey constrains the θ_{14} mixing angle with its $\bar{\nu}_e$ disappearance measurements while MINOS+ aims to constrain θ_{24} via the ν_μ disappearance mode. Predicted 90% C.L. sensitivities for MINOS+ combined with Bugey data are shown for exposures of 1.2×10^{21} POT

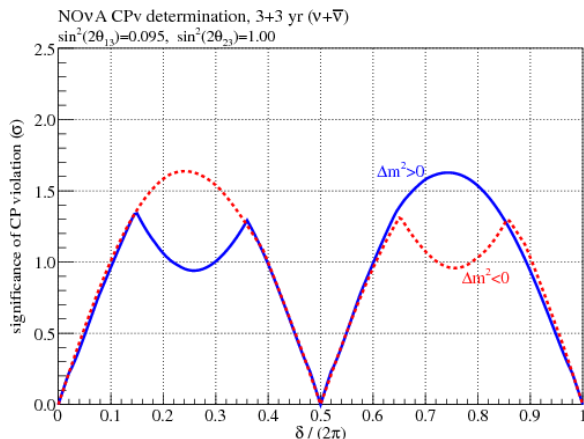


Figure 34. Significance of the determination that CP violation occurs in neutrino oscillations as a function of δ in standard deviations. These sensitivities are for NO ν A alone for the two possible orderings and $\sin^2(2\theta_{23}) = 1.0$. The significance goes to zero at $\delta = 0$ and $\delta = \pi$ since there is no CP violation at those points. The dips in the peaks occur because the mass ordering has not been resolved for the ordering containing the dips.

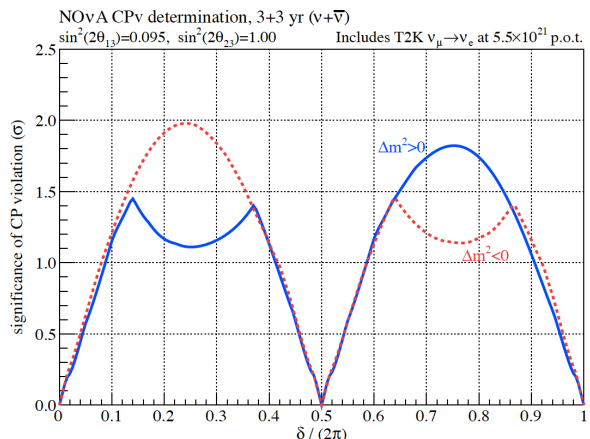


Figure 35. Same as the figure to the left except that information from the T2K experiment has been included.

in both neutrino-enhanced (left) and antineutrino-enhanced (right) NuMI beam configurations: these contours show that MINOS+ has the sensitivity to exclude substantial regions of parameter space allowed by MiniBooNE [86] and LSND [87] results.

In addition to searching for sterile neutrinos, MINOS+ will have a rich physics program that includes more precise measurements of $|\Delta m_{\text{atm}}^2|$ and $|\Delta \bar{m}_{\text{atm}}^2|$, a search for tau neutrinos, non-standard interactions, extra-dimensions, measurements of neutrino time-of-flight and atmospheric neutrinos.

8. Conclusion

Accelerator long-baseline experiments have made many measurements of neutrino oscillations, extracting fundamental neutrino mixing parameters and mass squared differences. The quantum mechanical interference pattern expected from neutrino oscillations has been observed with high statistics.

The most precise measurements to-date of $|\Delta m_{\text{atm}}^2|$ for both neutrinos and antineutrinos were made by a long-baseline neutrino oscillation experiment. Measurement of the largest neutrino mixing angle, θ_{23} , has reached the level of precision obtained using atmospheric neutrinos and second generation long-baseline experiments will soon improve the precision considerably further. Evidence for electron neutrino appearance in a beam of muon neutrinos has recently been obtained and is consistent with new results that demonstrate the disappearance of reactor electron antineutrinos due to θ_{13} .

Using a dedicated accelerator long-baseline experiment, candidate tau neutrino events have been directly observed in a beam of muon neutrinos and analysis of the complete data set is expected to reveal several more ν_τ candidates. Searches for oscillations into sterile neutrinos have set stringent limits on various models and these will improve further in the future. Long-baseline experiments have also been exploited in searches for Lorentz violation and to make

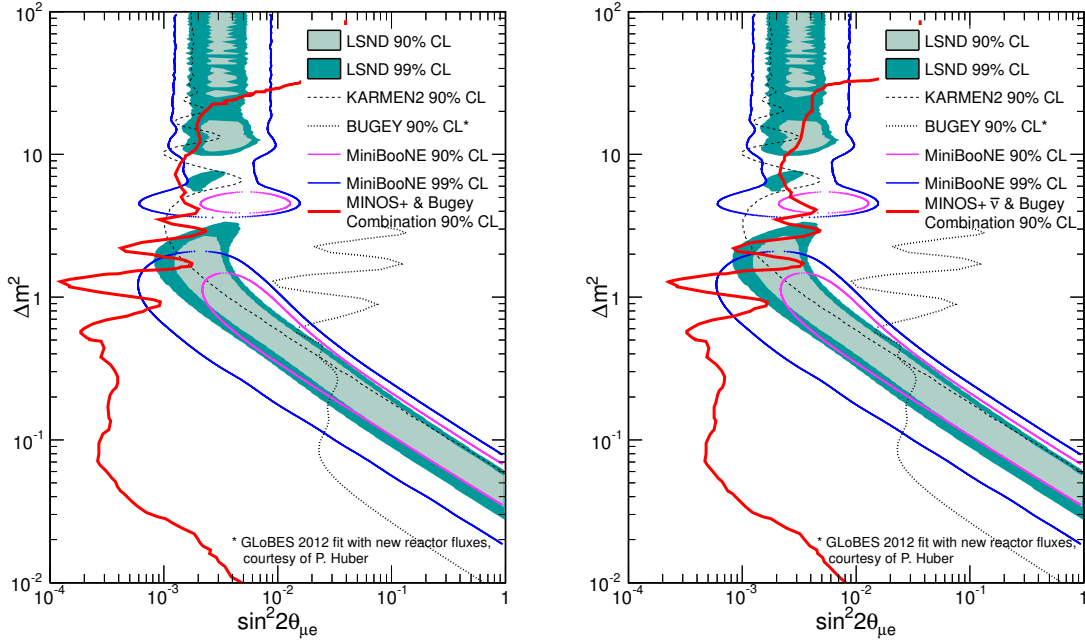


Figure 36. Expected sensitivities for MINOS+ combined with Bugey data to $\sin^2(2\theta_{\mu e})$ as relevant for sterile neutrino searches. 90% C.L. contours are shown for exposures of 1.2×10^{21} POT in both neutrino-enhanced (left) and antineutrino-enhanced (right) NuMI beam configurations [45]. The regions of parameter space allowed by MiniBooNE and LSND experiments along with the limits from KARMEN [88] are also shown.

world-leading measurements of the neutrino velocity.

The second generation long-baseline experiments currently taking data, or soon to start, will exploit the relatively large value of θ_{13} with the aim of measuring the mass hierarchy, determining the octant of θ_{23} , searching for CP violation and exploring models of new physics. Over the next decade, these experiments promise a rich program of research with the sensitivity to make fundamental discoveries.

9. References

- [1] M. Ieiri et al. . Proceedings of the 11th Symposium on Accelerator Science and Technology, SPring-8, Harima Science Garden City, Hyogo, Japan pages 377–379 (1997).
- [2] K. Anderson et al. The NuMI Facility Technical Design Report. FERMILAB-DESIGN-1998-01 (1998).
- [3] G. Acquistapace et al. The CERN neutrino beam to Gran Sasso (NGS). CERN-98-02, INFN-AE-98-05, CERN-YELLOW-98-02 (1998).
- [4] K. Abe et al. (T2K Collaboration). The T2K Experiment. Nucl.Instrum.Meth. **A659**, 106–135 (2011). 1106.1238.
- [5] M. Ahn et al. (K2K Collaboration). Measurement of Neutrino Oscillation by the K2K Experiment. Phys.Rev. **D74**, 072003 (2006). hep-ex/0606032.
- [6] I. Ambats et al. (MINOS Collaboration). The MINOS Detectors Technical Design Report (1998).
- [7] R. Acquafredda et al. The OPERA experiment in the CERN to Gran Sasso neutrino beam. JINST **4**, P04018 (2009).
- [8] F. Arneodo et al. (ICARUS). The ICARUS experiment, a second-generation proton decay experiment and neutrino observatory at the Gran Sasso Laboratory (2001). hep-ex/0103008.
- [9] K. Hirata et al. (KAMIOKANDE-II Collaboration). Experimental Study of the Atmospheric Neutrino Flux. Phys.Lett. **B205**, 416 (1988).

- [10] T. Haines et al. Calculation of Atmospheric Neutrino Induced Backgrounds in a Nucleon Decay Search. *Phys.Rev.Lett.* **57**, 1986–1989 (1986).
- [11] Y. Fukuda et al. (Super-Kamiokande Collaboration). Evidence for oscillation of atmospheric neutrinos. *Phys.Rev.Lett.* **81**, 1562–1567 (1998). [hep-ex/9807003](#).
- [12] M. Apollonio et al. (CHOOZ Collaboration). Search for neutrino oscillations on a long baseline at the CHOOZ nuclear power station. *Eur.Phys.J.* **C27**, 331–374 (2003). [hep-ex/0301017](#).
- [13] D. Ayres et al. Letter of Intent to build an Off-axis Detector to study ν_{μ} to ν_e oscillations with the NuMI Neutrino Beam (2002). [hep-ex/0210005](#).
- [14] D. Ayres et al. (NOvA Collaboration). NOvA: Proposal to build a 30 kiloton off-axis detector to study $\nu_{\mu} \rightarrow \nu_e$ oscillations in the NuMI beamline (2004).
- [15] D. Ayres et al. (NOvA Collaboration). The NOvA Technical Design Report. FERMLAB-DESIGN-2007-01 (2007).
- [16] Y. Abe et al. (Double Chooz Collaboration). Indication for the disappearance of reactor electron antineutrinos in the Double Chooz experiment. *Phys.Rev.Lett.* **108**, 131801 (2012).
- [17] F. An et al. (DAYA-BAY Collaboration). Observation of electron-antineutrino disappearance at Daya Bay. *Phys.Rev.Lett.* **108**, 171803 (2012). [1203.1669](#).
- [18] J. Ahn et al. (RENO collaboration). Observation of Reactor Electron Antineutrino Disappearance in the RENO Experiment. *Phys.Rev.Lett.* **108**, 191802 (2012). [1204.0626](#).
- [19] G. Tzanankos et al. (MINOS+ Collaboration). MINOS+: a Proposal to FNAL to run MINOS with the medium energy NuMI beam. FERMLAB-PROPOSAL-1016 (2011).
- [20] Y. Yamanoi et al. Large horn magnets at the KEK neutrino beamline. 2. *IEEE Trans.Appl.Supercond.* **10**, 252–255 (2000).
- [21] H. Noumi et al. GPS survey in long baseline neutrino-oscillation measurement. *IEEE Trans.Nucl.Sci.* **51**, 2245–2249 (2004).
- [22] R. M. Zwaska. *Accelerator systems and instrumentation for the NuMI neutrino beam*. Ph.D. thesis, University of Texas at Austin (2005).
- [23] A. I. Himmel. *Antineutrino Oscillations in the Atmospheric Sector*. Ph.D. thesis, Caltech (2011).
- [24] M. Meddahi et al. CERN Neutrinos to Gran Sasso (CNGS): Results from Commissioning. [oai:cds.cern.ch:1051376](#) (CERN-AB-2007-039), 4 p (2007).
- [25] N. Agafonova et al. (OPERA Collaboration). Observation of a first ν_{τ} candidate in the OPERA experiment in the CNGS beam. *Phys.Lett.* **B691**, 138–145 (2010). [1006.1623](#).
- [26] T. Ogitsu et al. Superconducting magnet system at the 50 GeV proton beam line for the J-PARC neutrino experiment. *IEEE Trans.Appl.Supercond.* **14**, 604–607 (2004).
- [27] T. Nakamoto et al. Design of superconducting combined function magnets for the 50GeV proton beam line for the J-PARC neutrino experiment. *IEEE Trans.Appl.Supercond.* **14**, 616–619 (2004).
- [28] T. Ogitsu et al. Operation of Superconducting Combined Function Magnet System for J-PARC Neutrino Beam Line. *Conf.Proc.* **C100523**, MOPEB033 (2010).
- [29] A. Suzuki et al. (K2K Collaboration). Design, construction, and operation of SciFi tracking detector for K2K experiment. *Nucl.Instrum.Meth.* **A453**, 165–176 (2000). [hep-ex/0004024](#).
- [30] T. Ishii et al. (K2K MRD GROUP). Near muon range detector for the K2K experiment: Construction and performance. *Nucl.Instrum.Meth.* **A482**, 244–253 (2002). [hep-ex/0107041](#).
- [31] K. Nitta, E. Aliu, S. Andringa, S. Aoki, S. Choi et al. The K2K SciBar detector. *Nucl.Instrum.Meth.* **A535**, 147–151 (2004). [hep-ex/0406023](#).
- [32] Y. Fukuda et al. (Super-Kamiokande Collaboration). The Super-Kamiokande detector. *Nucl.Instrum.Meth.* **A501**, 418–462 (2003).
- [33] D. Michael et al. (MINOS Collaboration). The Magnetized steel and scintillator calorimeters of the MINOS experiment. *Nucl.Instrum.Meth.* **A596**, 190–228 (2008). [0805.3170](#).
- [34] P. Adamson et al. The MINOS calibration detector. *Nucl.Instrum.Meth.* **A556**, 119–133 (2006).
- [35] A. Cabrera et al. (MINOS Collaboration). Comparisons of the MINOS Near and Far Detector Readout Systems at a Test Beam. *Nucl.Instrum.Meth.* **A609**, 106–113 (2009). [0902.1116](#).
- [36] C. Rubbia et al. Underground operation of the ICARUS T600 LAr-TPC: first results. *JINST* **6**, P07011 (2011). [1106.0975](#).
- [37] M. Ahn et al. (K2K Collaboration). Indications of neutrino oscillation in a 250 km long baseline experiment. *Phys.Rev.Lett.* **90**, 041801 (2003). [hep-ex/0212007](#).
- [38] D. Michael et al. (MINOS Collaboration). Observation of muon neutrino disappearance with the MINOS detectors and the NuMI neutrino beam. *Phys.Rev.Lett.* **97**, 191801 (2006).
- [39] N. Agafonova et al. (OPERA Collaboration). Search for $\nu_{\mu} \rightarrow \nu_{\tau}$ oscillation with the OPERA experiment in the CNGS beam. *New J.Phys.* **14**, 033017 (2012).
- [40] P. Adamson et al. (The MINOS Collaboration). Measurement of the neutrino mass splitting and flavor

- mixing by MINOS. *Phys.Rev.Lett.* **106**, 181801 (2011).
- [41] Y. Ashie et al. (Super-Kamiokande Collaboration). Evidence for an oscillatory signature in atmospheric neutrino oscillation. *Phys.Rev.Lett.* **93**, 101801 (2004).
- [42] Y. Ashie et al. (Super-Kamiokande Collaboration). A Measurement of atmospheric neutrino oscillation parameters by SUPER-KAMIOKANDE I. *Phys.Rev.* **D71**, 112005 (2005). [hep-ex/0501064](#).
- [43] P. Adamson et al. (MINOS Collaboration). A Study of Muon Neutrino Disappearance Using the Fermilab Main Injector Neutrino Beam. *Phys.Rev.* **D77**, 072002 (2008). [0711.0769](#).
- [44] P. Adamson et al. (MINOS Collaboration). Measurement of Neutrino Oscillations with the MINOS Detectors in the NuMI Beam. *Phys.Rev.Lett.* **101**, 131802 (2008). [0806.2237](#).
- [45] R. Nichol. Results from MINOS. Neutrino Conference Proceedings (2012).
- [46] P. Adamson et al. (MINOS Collaboration). Search for the disappearance of muon antineutrinos in the NuMI neutrino beam. *Phys.Rev.* **D84**, 071103 (2011). [1108.1509](#).
- [47] Y. Itow. Atmospheric Neutrinos: Results from running experiments. Neutrino Conference Proceedings (2012).
- [48] K. Abe et al. (T2K Collaboration). First Muon-Neutrino Disappearance Study with an Off-Axis Beam. *Phys.Rev.* **D85**, 031103 (2012).
- [49] P. Adamson et al. (MINOS collaboration). First direct observation of muon antineutrino disappearance. *Phys.Rev.Lett.* **107**, 021801 (2011). [1104.0344](#).
- [50] P. Adamson et al. (MINOS Collaboration). An improved measurement of muon antineutrino disappearance in MINOS. *Phys.Rev.Lett.* **108**, 191801 (2012). [1202.2772](#).
- [51] K. Abe et al. (Super-Kamiokande Collaboration). Search for Differences in Oscillation Parameters for Atmospheric Neutrinos and Antineutrinos at Super-Kamiokande. *Phys.Rev.Lett.* **107**, 241801 (2011).
- [52] M. Nakamura. Results from OPERA. Neutrino Conference Proceedings (2012).
- [53] K. Abe et al. (Super-Kamiokande Collaboration). A Measurement of atmospheric neutrino flux consistent with tau neutrino appearance. *Phys.Rev.Lett.* **97**, 171801 (2006). [hep-ex/0607059](#).
- [54] K. Abe et al. (Super-Kamiokande Collaboration). A Measurement of the Appearance of Atmospheric Tau Neutrinos by Super-Kamiokande (2012). [1206.0328](#).
- [55] M. Ahn et al. (K2K Collaboration). Search for electron neutrino appearance in a 250 km long baseline experiment. *Phys.Rev.Lett.* **93**, 051801 (2004). [hep-ex/0402017](#).
- [56] S. Yamamoto et al. (K2K Collaboration). Improved search for $\nu_\mu \rightarrow \nu_e$ oscillation in a long-baseline accelerator experiment. *Phys.Rev.Lett.* **96**, 181801 (2006).
- [57] P. Adamson et al. (MINOS Collaboration). Search for muon-neutrino to electron-neutrino transitions in MINOS. *Phys.Rev.Lett.* **103**, 261802 (2009). [0909.4996](#).
- [58] P. Adamson et al. (The MINOS Collaboration). New constraints on muon-neutrino to electron-neutrino transitions in MINOS. *Phys.Rev.* **D82**, 051102 (2010). [1006.0996](#).
- [59] P. Adamson et al. (MINOS Collaboration). Improved search for muon-neutrino to electron-neutrino oscillations in MINOS. *Phys.Rev.Lett.* **107**, 181802 (2011). [1108.0015](#).
- [60] K. Abe et al. (T2K Collaboration). Indication of Electron Neutrino Appearance from an Accelerator-produced Off-axis Muon Neutrino Beam. *Phys.Rev.Lett.* **107**, 041801 (2011). [1106.2822](#).
- [61] N. Abgrall et al. (NA61/SHINE Collaboration). Measurements of Cross Sections and Charged Pion Spectra in Proton-Carbon Interactions at 31 GeV/c. *Phys.Rev.* **C84**, 034604 (2011). [1102.0983](#).
- [62] N. Abgrall et al. (NA61/SHINE Collaboration). Measurement of Production Properties of Positively Charged Kaons in Proton-Carbon Interactions at 31 GeV/c. *Phys.Rev.* **C85**, 035210 (2012). [1112.0150](#).
- [63] T. Nakaya. Results from T2K. Neutrino Conference Proceedings (2012).
- [64] P. Adamson et al. (MINOS Collaboration). Search for active neutrino disappearance using neutral-current interactions in the MINOS long-baseline experiment. *Phys.Rev.Lett.* **101**, 221804 (2008). [0807.2424](#).
- [65] P. Adamson et al. (The MINOS Collaboration). Search for sterile neutrino mixing in the MINOS long baseline experiment. *Phys.Rev.* **D81**, 052004 (2010). [1001.0336](#).
- [66] S. Fukuda et al. (Super-Kamiokande Collaboration). Tau neutrinos favored over sterile neutrinos in atmospheric muon-neutrino oscillations. *Phys.Rev.Lett.* **85**, 3999–4003 (2000). [hep-ex/0009001](#).
- [67] P. Adamson et al. (MINOS Collaboration). Active to sterile neutrino mixing limits from neutral-current interactions in MINOS. *Phys.Rev.Lett.* **107**, 011802 (2011). [1104.3922](#).
- [68] P. Adamson et al. (MINOS Collaboration). Measurement of neutrino velocity with the MINOS detectors and NuMI neutrino beam. *Phys.Rev.* **D76**, 072005 (2007).
- [69] G. R. Kalbfleisch, N. Baggett, E. C. Fowler, and J. Alspector. Experimental Comparison of Neutrino, Antineutrino, and Muon Velocities. *Phys. Rev. Lett.* **43**, 1361–1364 (1979). URL <http://link.aps.org/doi/10.1103/PhysRevLett.43.1361>.
- [70] T. Adam et al. (OPERA Collaboration). Measurement of the neutrino velocity with the OPERA detector in the CNGS beam (2011). [1109.4897](#).

- [71] M. Antonello et al. (ICARUS Collaboration). Measurement of the neutrino velocity with the ICARUS detector at the CNGS beam. *Phys.Lett.* **B713**, 17–22 (2012). 1203.3433.
- [72] P. Alvarez Sanchez et al. (Borexino Collaboration). Measurement of CNGS muon neutrino speed with Borexino. *Phys.Lett.* **B716**, 401–405 (2012). 1207.6860.
- [73] N. Y. Agafonova et al. (LVD Collaboration). Measurement of the velocity of neutrinos from the CNGS beam with the Large Volume Detector. *Phys.Rev.Lett.* **109**, 070801 (2012). 1208.1392.
- [74] P. Adamson. Neutrino Speed: Results and prospects of experiments at other beamlines. *Neutrino Conference Proceedings* (2012).
- [75] D. Colladay and V. A. Kostelecky. CPT violation and the standard model. *Phys.Rev.* **D55**, 6760–6774 (1997). [hep-ph/9703464](#).
- [76] D. Colladay and V. A. Kostelecky. Lorentz violating extension of the standard model. *Phys.Rev.* **D58**, 116002 (1998). [hep-ph/9809521](#).
- [77] V. A. Kostelecký. Gravity, Lorentz violation, and the standard model. *Phys. Rev. D* **69**, 105009 (2004). URL <http://link.aps.org/doi/10.1103/PhysRevD.69.105009>.
- [78] P. Adamson et al. (MINOS Collaboration). Testing Lorentz Invariance and CPT Conservation with NuMI Neutrinos in the MINOS Near Detector. *Phys.Rev.Lett.* **101**, 151601 (2008). 0806.4945.
- [79] P. Adamson et al. (The MINOS Collaboration). Search for Lorentz invariance and CPT violation with muon antineutrinos in the MINOS Near Detector. *Phys.Rev.* **D85**, 031101 (2012).
- [80] P. Adamson et al. (MINOS Collaboration). A Search for Lorentz Invariance and CPT Violation with the MINOS Far Detector. *Phys.Rev.Lett.* **105**, 151601 (2010). 1007.2791.
- [81] V. A. Kostelecky and N. Russell. Data Tables for Lorentz and CPT Violation. *Rev.Mod.Phys.* **83**, 11 (2011).
- [82] T. Ajima et al. Tokai-to-Kamioka (T2K) Long Baseline Neutrino Oscillation Experiment Proposal (2006). URL http://j-parc.jp/researcher/Hadron/en/pac_0606/pdf/p11-Nishikawa.pdf.
- [83] Y. Abe et al. (Double Chooz Collaboration). Reactor electron antineutrino disappearance in the Double Chooz experiment. *Phys.Rev.* **D86**, 052008 (2012). 1207.6632.
- [84] D. Dwyer. Improved Measurement of Electron-antineutrino Disappearance at Daya Bay. *Neutrino Conference Proceedings* (2012).
- [85] Y. Declais et al. Search for neutrino oscillations at 15-meters, 40-meters, and 95-meters from a nuclear power reactor at Bugey. *Nucl.Phys.* **B434**, 503–534 (1995).
- [86] A. Aguilar-Arevalo et al. (MiniBooNE Collaboration). Event Excess in the MiniBooNE Search for $\bar{\nu}_\mu \rightarrow \bar{\nu}_e$ Oscillations. *Phys.Rev.Lett.* **105**, 181801 (2010). 1007.1150.
- [87] A. Aguilar-Arevalo et al. (LSND Collaboration). Evidence for neutrino oscillations from the observation of anti-neutrino(electron) appearance in a anti-neutrino(muon) beam. *Phys.Rev.* **D64**, 112007 (2001). [hep-ex/0104049](#).
- [88] B. Armbruster et al. (KARMEN Collaboration). Upper limits for neutrino oscillations $\bar{\nu}_\mu \rightarrow \bar{\nu}_e$ from muon decay at rest. *Phys.Rev.* **D65**, 112001 (2002). [hep-ex/0203021](#).